

Department of Physics and Astronomy
University of Heidelberg

Diploma thesis
in Physics

submitted by
Philipp Simon
born in Bielefeld
2010

Apparatus for the preparation of ultracold Fermi gases

This diploma thesis has been carried out by Philipp Simon
at the
Physikalisches Institut Heidelberg
and the
Max-Planck-Institute for Nuclear Physics
under the supervision of
Professor Selim Jochim

Abstract:

This thesis reports on the first steps towards an experimental setup capable of realizing an ultracold three-component Fermi gas in an optical lattice: the construction of an apparatus that captures and cools ${}^6\text{Li}$ -atoms inside a magneto optical trap (MOT).

The focus of this thesis was the implementation of the Zeeman slower, the laser system and hard- and software controlling the experiment. Since these provide the starting point for all future developments it was especially important to ensure that they do not limit future experiments.

With a MOT loading rate of $L \approx 3 \cdot 10^8$ atoms/second at an oven temperature of 350°C it is possible to capture enough atoms for further experiments in about one second allowing fast cycle times of the experiment.

The achieved background pressure in the vacuum chamber, essential for the next experimental steps, is excellent as indicated by the background gas collision limited MOT lifetime of $\tau \approx 23$ minutes.

The next step will be to implement a dipole trap to further cool the ${}^6\text{Li}$ -atoms.

Zusammenfassung:

Diese Diplomarbeit beschreibt den Aufbau eines Experiments zur Untersuchung von ultrakalten dreikomponentigen Fermigasen in einem optischen Gitter. Der erste Schritt war die Konstruktion eines Apparates, der ${}^6\text{Li}$ Atome in einer magneto-optischen Falle einfangen und kühlen kann.

Der Fokus dieser Arbeit war die Realisierung und Charakterisierung des Zeeman Abbremsers, des dafür benötigten Lasersystems und der Hard- und Software die das Experiment kontrolliert. Da diese die Grundlage für alle weiteren Experimente bilden, ist es von besonderer Wichtigkeit sicherzustellen, dass sie weitere Entwicklungen nicht limitieren.

Durch MOT Laderaten von $L \approx 3 \cdot 10^8$ Atomen/Sekunde bei Ofentemperaturen von 350°C ist es möglich in einer Sekunde genug Atome für weitere Experimente einzufangen, sodass die Experimentzyklen nicht von der Laderate limitiert werden.

Der erreichte Druck in der Vakuumkammer, der essenziell für die nächsten experimentellen Schritte sein wird, ist exzellent, wie durch die Restgaskollisionen limitierte MOT Lebensdauer von $\tau \approx 23$ Minuten deutlich wurde.

Der nächste Schritt wird der Aufbau einer Dipolfalle sein, um die ${}^6\text{Li}$ -Atome weiter abzukühlen.

Contents

1	Introduction	1
2	Ultracold Fermi Gases	5
3	Tools of the trade	9
3.1	Resources	9
3.1.1	Lithium 6 Atoms	9
3.1.2	Magnetic Fields	10
3.1.3	Light	10
3.2	Interactions	13
3.2.1	Atom Light Interaction	13
3.2.2	Atom Magnetic-field Interaction	17
3.3	Laser Cooling	19
3.3.1	Zeeman slower	21
3.3.2	Magneto Optical Trap	23
4	Experiment	31
4.1	Vacuum Chamber	31
4.2	Experimental Control	33
4.3	Cooling and Trapping	36
4.3.1	Lithium 6 System	36
4.3.2	Optical Setup	40
4.3.3	Zeeman slower	43
4.3.4	MOT	53
5	Conclusion and Outlook	61
	Bibliography	65

1 Introduction

The constituent parts of all matter known today are fermions. By definition a fermion is a particle, fundamental or composite, that obeys the Fermi-Dirac statistics. These state that two identical fermions can not occupy the same quantum state at any time. It turns out that all observed fermions have a half-integer spin as opposed to their counterpart - the bosons - that have an integer spin and obey the Bose-Einstein statistics. Common examples of fermions are of course the electron which is a fundamental particle and the proton and neutron which are in fact composite particles consisting of three quarks that are fermions by themselves.

These fundamental principles of quantum mechanics and their consequences make fermionic systems a very rich topic of research.

While fermionic systems can be studied in solid state physics or in nuclear physics both fields have to deal with very complex systems that are only partially controllable and observable.

In recent years an almost perfect system to study fermionic systems came into reach of experimentalists. Dilute gases of ultracold fermionic atoms offer unprecedented control over experimental parameters as well as great observability. By using these dilute gases one can (to a certain extent) break down complex systems and form simulators, that have all the important properties of the original system while lacking their massive complexity. Additionally, by using techniques from atomic physics, one gains an almost perfect control over all parameters of the experiment and great observability.

A major technical challenge in realizing these simulators has been the achievable level of quantum degeneracy. A measure for this is the phase space density $\rho = n\lambda_{dB}^3$ which is the product of the density n and the de Broglie wavelength λ_{dB} of the particle. To reach quantum degeneracy one has to achieve phase space densities of the order $\rho \approx 1$ which means that the de Broglie wavelength is in the order of the interparticle spacing. In this regime the commonly used measure of degeneracy is the fraction T/T_F where T_F is the Fermi temperature. To make dilute gases display the quantum behavior of the fermionic system it has to be cooled to very low temperatures (order of nK). Doing so requires laser systems and techniques that only became feasible in recent years.

The first step was done in 1986 when magneto-optical trapping of neutral atoms

was realized for the first time [Chu86]. This provided experimentalists with a dilute gas at temperatures on the order of μK . While this corresponds to phase space densities seven orders of magnitude above room temperature gases it is still far from degeneracy. Nevertheless the technique remains the starting point of all further experiments. It took another 10 years to realize the first degenerate quantum gas.

In 1995 E.A. Cornell, C.A. Wieman [And95] and W. Ketterle [Dav95] cooled bosons to degeneracy realizing a phase of matter which had been predicted 80 years before [Ein25] [Bos24], the so-called Bose-Einstein condensate. This experimental breakthrough was awarded with the Nobel prize in 2001. The first degenerate fermionic system was reached in 1999 by D.S. Jin [Jin99] with $T/T_F \approx 0.5$. Deeper degeneracies were reached using new cooling techniques in 2001 by R.G. Hulet [Tru01] with $T/T_F \approx 0.2$.

The next big step was the application of so called Feshbach resonances [Ste99] that provide control over the interaction between the atoms. It is important to note that the interaction conveyed by these resonances is detached from the underlying system's properties (i.e. which atoms are used).

At this point one could prepare a system of fermions that are isolated from external influences, can be controlled and observed very precisely at the same time. For example the spin orientation can be changed by applying external radio-frequency fields and the trapping potential can be shaped in a number of ways using different laser setups. The system can be observed during the entire process allowing in depth analysis of the properties and dynamics of the quantum system.

These tools enabled breakthrough experiments by C.A. Regal [Reg03], M. Greiner [Gre03], S. Jochim [Joc03] and M. W. Zwierlein [Zwi03] in 2003. By tuning the scattering length to large positive values the fermionic atoms paired into bosonic molecules that were subsequently cooled into a Bose-Einstein condensate. For negative scattering lengths on the other hand the attractive meanfield interaction allows the formation of weakly bound Cooper pairs in momentum space. These now directly observable pairs are the core of the first microscopic theory of superconductivity formulated in 1957 by J. Bardeen and L.N. Cooper [Bar57].

In recent years experiments with periodic trapping potentials have made huge progress. These systems provide a superb simulator for the Hubbard model [Hub63] which is used to describe an electron gas in crystal structures. One effect predicted by this model is the Mott insulator [Mot90], in which suppression of conductivity is induced by interaction rather than a filled Bloch band. This system was first realized with fermions by R. Jordens and N. Strohmaier in 2008 [Jor08]. Closely related to this phase are the effects of high temperature superconductivity [Lee06] and superfluidity [Hof02].

Our work aims to build an apparatus that implements a ultracold Fermi gas of

^6Li in a 2-D optical lattice and an imaging system with almost single site resolution to explore these and other physics. This thesis will present the first steps towards realizing these goals. We will start by reviewing some general theories of ultracold Fermi gases in chapter 2. In chapter 3 we will describe the fundamental tools we need to build an atom trap. We will review the basic interactions involved and explain the principles of lasercooling. In chapter 4 we will turn to the real life system and outline some design decisions especially regarding the Zeeman slower and the laser setup. In this chapter we will also describe how we built the apparatus and present first results of the apparatus regarding the effectiveness of the trapping setup. In chapter 5 a outlook onto the next steps will be given.

2 Ultracold Fermi Gases

In this chapter we will summarize the basics of particle statistics and the interactions of ultracold gases. After presenting some generic theory we will take a brief look at our ${}^6\text{Li}$ system and its properties.

Quantum Statistics

In general all particles are subject to the following distribution regarding their energy or momentum respectively:

$$n_i = \frac{g_i}{e^{(\epsilon_i - \mu)/k_B T} + D} \quad (2.1)$$

where n_i is the number of particles in state i , g_i is the degeneracy, ϵ_i is the energy, μ the chemical potential and T the temperature. The parameter D can take three different values which dramatically change the behavior of the particles.

- For $D = 0$ it is called **Maxwell-Boltzmann distribution** and describes classical particles like an ideal gas.
- For $D = -1$ it is called **Bose-Einstein distribution** and describes the quantum statistics of bosons.
- For $D = 1$ it is called **Fermi-Dirac distribution** and describes the quantum statistics of our fermions.

For a Fermi gas with $T = 0$ this becomes:

$$n(\mathbf{r}, \mathbf{p}) = \begin{cases} g_i & ; \epsilon_i < \mu \\ 0 & ; \epsilon_i > \mu \end{cases} \quad (2.2)$$

The energy levels ϵ_i of the trapping potential $V(\mathbf{r})$ are filled by exactly one fermion per state up to the chemical potential. For higher temperatures the distribution is not a sharp step anymore but gets smeared out more and more. For a 3-dimensional harmonic trapping potential

$$V(\mathbf{r}) = \frac{1}{2}m(\omega_x^2 x^2 + \omega_y^2 y^2 + \omega_z^2 z^2)$$

with a mean trapping frequency $\bar{\omega} = \sqrt[3]{\omega_x \omega_y \omega_z}$ and N fermions in the trap we can define the **Fermi energy**:

$$E_F = \hbar \bar{\omega} \sqrt[3]{6N} \quad (2.3)$$

which corresponds to the highest occupied state. More information on this topic can be found in [Ket08].

Ultracold Scattering

The interaction between neutral ultracold atoms is conveyed by elastic collisions. If we apply quantum mechanical scattering theory [NoI06] and assume our atoms to be fermions at low energy ($T \leq 1$ mK for ${}^6\text{Li}$), so that only s-wave scattering is important, we get the following results for the total cross section:

$$\sigma_{\text{non identical}} = \frac{4\pi a^2}{1 + k^2 a^2} \quad (2.4)$$

$$\sigma_{\text{identical}} = 0 \quad (2.5)$$

where a is the scattering length and k is the momentum of the fermion. From these results we can learn two very important facts:

1. A Fermi gas of identical fermions does not interact via scattering, which means in the case of a spin polarized neutral ${}^6\text{Li}$ gas that it does not interact at all. To introduce an interaction into the system we have to use a mixture of spin states of ${}^6\text{Li}$, so that there are non-identical fermions in the sample.
2. The scattering process does not depend on the details of the scattering potential which makes it, over a broad range of a , **universal**. Meaning that results obtained in ${}^6\text{Li}$ experiments can be carried over to other problems where the details of the scattering potential are irrelevant and only a describes the interaction. It turns out that many effects can be understood in this framework like the afore mentioned superfluidity or superconductivity.

Tuning the Scattering Length

One of the most important properties of ultracold Fermi gases is that the scattering length a can be tuned to arbitrary values by applying external homogeneous magnetic fields B . This phenomenon is called **Feshbach resonance** after H. Feshbach who first described this effect in the framework of nuclear physics [Fes58]. A detailed analysis of this effect [Moe95] shows that the scattering length a behaves like:

$$a(B) = a_{bg} \left(1 - \frac{\Delta}{B - B_0} \right) \quad (2.6)$$

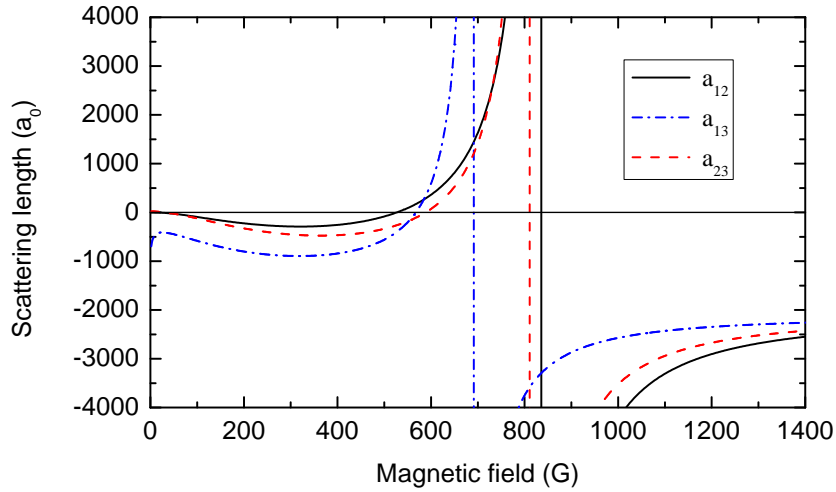


Figure 2.1: Scaling of the scattering length between the three hyperfine levels (in units of Bohr's radius) of ${}^6\text{Li}$ with the external magnetic field.

with a background scattering rate a_{bg} close to the resonance B_0 . Figure 2.1 shows Feshbach resonances between ${}^6\text{Li}$ atoms in different spin states.

3 Tools of the trade

Since we want to prepare quantum systems of ultracold atoms in an exact and reproducible way we will need tools that allow for a high level of control. In this chapter we will take a look at the experimental tools and methods which provide that needed level of control. First we need a mechanism to capture and cool atoms. Since atoms do not do that by themselves we will need to force them to. The only feasible fundamental force at our disposal is of course the electro-magnetic force. Of special interest are the influence of static magnetic fields on the atomic energy levels and the response of atoms to electro-magnetic radiation. So we will start by reviewing some properties of the atom-light and atom-magnetic-field interaction. Next we will turn to the experimental techniques and the sources of the electro-magnetic force (light and magnetic-field) and atoms. In the last step we will combine the knowledge of the interactions with the appropriate sources to construct an effective cooling and trapping mechanism.

3.1 Resources

In this chapter we will describe the sources of our basic ingredients, namely: atoms, magnetic fields and light. We will need all of them to realize our trapping setup.

3.1.1 ${}^6\text{Li}$ Atoms

The sources of atoms are in our case small chunks of ${}^6\text{Li}$ (about 1 gram) placed in an oven. With a temperature of $T = 350\text{ }^\circ\text{C}$, vapor pressure $p = 1.33 \cdot 10^{-5}$ mbar, mean velocity $\bar{v} = \sqrt{\frac{8kT}{\pi m}} \approx 1500$ m/s and oven aperture $A = (5\text{mm})^2\pi$ we can get an estimation of the total flux (taken from [Sav98])

$$f_{\text{oven}} = \frac{p\bar{v}A}{4kT} \approx 10^{16} \frac{\text{atoms}}{\text{sec}} . \quad (3.1)$$

The velocity distribution of the beam is of course a Maxwell-Boltzmann distribution. With this amount of ${}^6\text{Li}$ and temperature we should be able to operate the oven for about 20 000 hours.

3.1.2 Magnetic Fields

As Maxwell's laws tell us a magnetic field is generated by letting an electric current flow. The easiest way to do that is a simple copper wire usually wound into a coil. The resulting magnetic field can be calculated using Biot Savart's law. The actual fields usually match the calculated fields with very good precision without having to use special winding techniques, as the size of the coils is much larger than the atom sample. A configuration that is found in almost every setup in the field of atom physics is the **Helmholtz configuration**. It can be achieved by placing two coils of radius R exactly that radius apart. Hereby the non-uniformity of the field at the center of the coils is minimized. The magnetic field B along the radial direction becomes

$$B = \left(\frac{4}{5}\right)^{3/2} \frac{\mu_0 n I}{R} \quad (3.2)$$

where μ_0 is the permeability constant, I the current and n the number of windings.

The achievable field strength is limited by the power dissipation $P = I^2 R$ and thus by the applied cooling. In our setup we will use water cooled heat sinks to allow relatively high fields at manageable technical complexity. Another complication are hysteresis effects. We generally want our field to be exactly the same for each experimental realization. Therefore materials with low magnetic susceptibility μ are used in parts that are exposed to magnetic fields.

3.1.3 Light

The source of light we will use has to meet very high requirements regarding intensity, stability and tuneability as described in chapter 3.2.1. The only source that has a chance to fulfill them is a laser. Not so long ago this would have required building that laser yourself at great cost of money and time. Luckily the recent technological advances in laser technology made that job much easier (the manufacturing process of standard laser diodes used in consumer electronics like DVD players is essentially the same as the one needed for our lasers). Therefore laser systems with the needed properties have become commercially available. What we will use is a Toptica TA Pro solid state laser (see table 3.1 for specifications). We will not discuss the mode of operation of diode lasers here, there are however some secondary sources we will discuss shortly. They do not emit light by themselves but change the properties of incident light in a way that they can be described as sources themselves.

Max. power at 671 nm	350 mW
mode-hop free tuning range	≈ 3 GHz
Linewidth	≈ 100 kHz
Polarization	linear $> 100 : 1$

Table 3.1: Specifications of our Toptica TA Pro. The linewidth is well below the natural linewidth of the used transitions (see chapter 4.3.1).

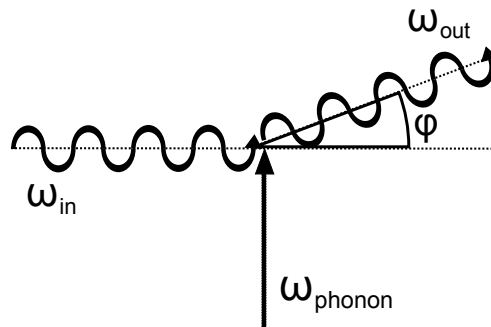


Figure 3.1: Simplified picture of the photon-phonon interaction.

Accusto-Optical Modulator

The first example is the **accusto-optical modulator** (or short AOM). To understand this we will take a very brief look into the light-sound interaction. Sound is not a fundamental force or particle like magnetic fields or atoms but rather a periodic pressure fluctuation of a medium. In our case the medium is an optically transparent crystal. It is known from solid state physics that sound waves in solids can be described in the phonon picture where phonons are the quanta of the oscillation of the crystal lattice. In a very simple model we can describe the light-sound interaction as an absorption of a phonon by a photon. By absorbing a phonon with $\mathbf{p}_{\text{phonon}} = \hbar\mathbf{k}_{\text{phonon}}$ the photon changes its own momentum and therefore its direction and frequency. The process is schematically shown in figure 3.1. By absorbing different numbers N of phonons the incident beam is deflected into several new beams each with the frequency $\omega_{\text{out}} = \omega_{\text{in}} + N\omega_{\text{phonon}}$ and deflection angle $\sin(\theta) = \frac{N\lambda}{2\Lambda}$ where λ is the wavelength of the light in the medium and Λ the wavelength of the sound wave. To introduce the oscillation into the crystal mechanical stress is applied through a piezo crystal driven by a radio frequency (or short rf) signal. Typical frequencies range from MHz to a few GHz. The limit of this effect is the sound velocity in the crystal

and also the mechanical stress it can take.

For our purposes it is sufficient to know that we can shift our laser's frequency in the range of 100 MHz freely without having to manipulate the laser itself (for more details see [Sal91]).

Since rf signals can be switched on and off very fast an AOM can also be used as a fast optical switch (meaning much faster than mechanical shutters). As soon as the rf power is off the beam returns to its undeflected path which can for example lead to a beam dump to turn the beam off entirely.

Optical Fiber

Another very useful tool are optical fibers. By using a very thin (μm scale) glass cylinder with refractive index n_1 cladded with a second glass with a slightly lower refractive index $n_2 < n_1$ light can be guided along the fiber. To understand this we can use simple geometry optics. Total refraction occurs when the angle with the fiber axes is lower than the critical angle

$$\tilde{\theta}_c = \pi/2 - \theta_c \cos^{-1}(n_2/n_1) .$$

To successfully couple a beam into the fiber the angle with the fiber axes θ after the initial air to core material refraction needs to be smaller than θ_c . Applying Snell's law yields

$$\theta_a = \sin^{-1} NA \tag{3.3}$$

where

$$NA = \sqrt{n_1^2 - n_2^2} \tag{3.4}$$

is the numerical aperture of the fiber. By making the core radius of the fiber small enough a single mode fiber can be created. In this kind of fiber only the fundamental mode LP_{01} is transmitted (see [Sal91] for a more complete discussion). So whatever the beam we couple into the single mode fiber looks like only a Gaussian like profile will remain at the exit. Of course this will cost us light intensity because all other modes are lost.

Therefore fibers have two very useful properties. They are very convenient to guide the light from where it is generated (the optical table) to where it is needed (the vacuum chamber). And second they clear the beam profile of any irregularities.

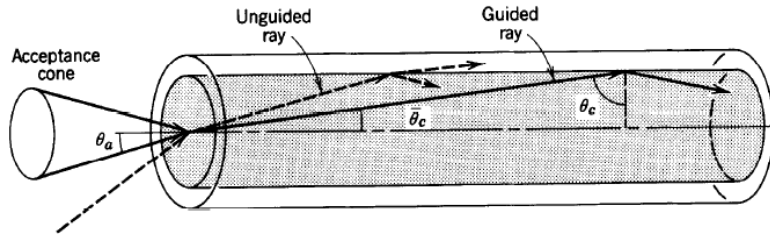


Figure 3.2: Geometry of a simple stepped index fiber (taken from [Sal91])

3.2 Interactions

In this chapter we will review the most important concepts and results of the atom-light and atom-magnetic-field interaction. This will help us to understand the more complex cooling and trapping mechanism which we will construct later from these basic interactions. We will start each chapter with some general theoretical formalisms. In the next step we apply them to the system at hand to get a feeling for the relevant numbers.

3.2.1 Atom Light Interaction

First we will consider the interaction between light and an atom. Here we will follow the discussion of [Met99]. To keep things simple we will assume the light to be a (nearly) monochromatic plane wave. This restriction is very well met by a laser (discussed in 3.1.3). Since we use monochromatic light it is also valid to represent our atom by a two level system. In the following we will denote the levels with $|g\rangle$ for the ground state and $|e\rangle$ for the excited state.

The Interaction Hamiltonian

The Hamiltonian $\hat{H}'(t)$ of the interaction is given by

$$\hat{H}'(t) = -e\mathbf{E}(\mathbf{r}, t) \cdot \hat{\mathbf{r}} \quad (3.5)$$

where \mathbf{E} is the electric component of the light which interacts with the dipole moment $\boldsymbol{\mu} = -e\mathbf{r}$ of the atom. Luckily this interaction imposes only a very small perturbation on the central field Hamiltonian, which describes the unperturbed atom. This can be easily shown by comparing the electric field strength of the nucleus at the location of the electron

$$E_{\text{nuc}} = \frac{1}{4\pi\epsilon_0} \frac{e}{a_0} \approx 10^{11} \text{ V/m}$$

3.2 Interactions

with the one of a light field with typically mW/cm^2 intensity

$$E_{\text{light}} = \sqrt{\frac{2I}{c\epsilon_0}} \approx 1 \text{ V/m} .$$

Applying the time dependent Schrödinger equation leads to the the following expressions for the amplitudes $c_{e,g}$ of the respective states:

$$i\hbar \frac{dc_g(t)}{dt} = c_e(t) \hat{H}'(t)_{ge} e^{-i\omega_0 t} \quad (3.6)$$

$$i\hbar \frac{dc_e(t)}{dt} = c_g(t) \hat{H}'(t)_{eg} e^{-i\omega_0 t} \quad (3.7)$$

where ω_0 is the atomic resonance frequency. Now we have to specify the electric field \mathbf{E} to be a traveling plane wave of frequency ω :

$$\mathbf{E}(\mathbf{r}, t) = E_0 \boldsymbol{\epsilon} \cos(kz - \omega t) \quad (3.8)$$

where E_0 is the amplitude of the light field and $\boldsymbol{\epsilon}$ is the unit polarization. Putting equations 3.5 and 3.8 together leads to

$$\hat{H}'_{eg}(t) = \hbar\Omega \cos(kz - \omega t) . \quad (3.9)$$

The atom-light interaction is thus described by one parameter, the **Rabi frequency**:

$$\Omega \equiv -\frac{eE_0}{\hbar} \langle e | \hat{\mathbf{r}} | g \rangle . \quad (3.10)$$

This Rabi frequency indicates how strongly the two states with dipole moment $-e\langle e | \hat{\mathbf{r}} | g \rangle$ are coupled. Because of this coupling the amplitudes of the ground and excited state are oscillating with exactly this frequency Ω . The Hamiltonian can also be put in matrix form

$$\hat{H} = \frac{\hbar}{2} \begin{bmatrix} -2\delta & \Omega \\ \Omega & 0 \end{bmatrix} \quad (3.11)$$

with the detuning $\delta = \omega - \omega_0$. So far the equations describe the absorption and induced emission of light where both processes do not affect the light field itself even though photons are removed from or added to it. Also the effect of spontaneous emission that effectively removes photons from the system (as they are emitted in random directions) is entirely neglected. This simple model however instructive to understand the basic principles of atom light interaction does not describe our system in the needed detail.

The Optical Bloch equations

The problems mentioned above can be handled semi-classical by introducing the density matrix to describe the mixed system which will lead to so called **optical Bloch equations**, where spontaneous emission is inserted “by hand” as a dampening term (see [CT08]). The alternative would be a full quantum-electro-dynamic description (see [Gre92]).

Since the complete derivation of the optical Bloch equations is beyond the scope of this work we will just skip forward to their results. The most important result is the occupation probability of the excited state

$$p_{ee} = \frac{s_0/2}{1 + s_0 + (2\delta/\gamma)^2} \quad (3.12)$$

with the spontaneous decay rate γ (which is basically the inverse life time of the excited state i.e. $\gamma = 2\pi \cdot 5.87$ MHz for ${}^6\text{Li}$) and the on-resonance saturation parameter

$$s_0 \equiv \frac{2|\Omega|^2}{\gamma^2} = \frac{I}{I_S} .$$

The on-resonance saturation leads to a broadening of the linewidth of the resonance as the power of the light increases. It can be expressed in terms of the saturation intensity which is $I_S = 2.54$ mW/cm² for the cooling transition in our ${}^6\text{Li}$ system.

The process we are interested in is the absorption of a photon from the beam and the subsequent spontaneous emission. The frequency of this process is called scattering rate Γ_{sc} . With the formulas at hand the calculation becomes straight forward as we simply have to multiply the rate of spontaneous decay from the excited state with the probability to be in the excited state (3.12).

$$\Gamma_{sc} = \gamma p_{ee} = \frac{s_0\gamma/2}{1 + s_0 + (2\delta/\gamma)^2} . \quad (3.13)$$

In figure 3.3 the effect of different detunings and saturations on this scattering rate are displayed.

The Spontaneous Force

Let us now turn to the force that is conveyed by the process of absorption and spontaneous emission. Since the force is the time derivative of the momentum we take a look at the momentum balance of N absorption/emission processes.

$$\mathbf{F}_{sp} = \frac{d}{dt} (\langle \hbar \mathbf{k}_{\text{abs}} \rangle_N + \langle \hbar \mathbf{k}_{\text{spont}} \rangle_N)$$

3.2 Interactions

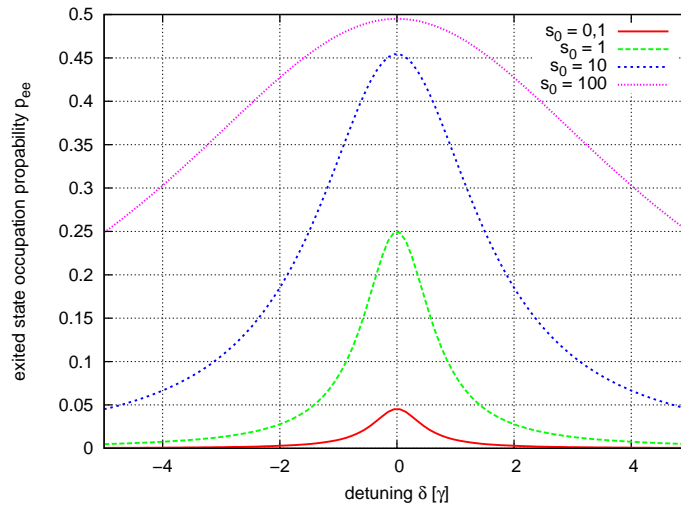


Figure 3.3: Scattering rate Γ_{sc} as function of detuning δ for different saturation parameters s_0 . Note that the natural linewidth γ broadens to $\gamma' = \gamma\sqrt{1 + s_0}$ from power broadening.

Since the spontaneous emission occurs in random directions the mean momentum transfer over many spontaneous emissions becomes zero. The absorbed photons on the other hand all came with the same \mathbf{k}_{abs} . Together with the scattering rate they add up to:

$$F_{sp} = \hbar k_{\text{abs}} \Gamma_{sc} = \frac{\hbar k_{\text{abs}} s_0 \gamma / 2}{1 + s_0 + (2\delta/\gamma)^2} . \quad (3.14)$$

This force is called the **spontaneous force**. The maximal force is reached for $\delta = 0$ and a saturation parameter $s_0 \gg 1$:

$$F_{max} = \frac{\hbar k \gamma}{2} .$$

If we plug in the numbers for ${}^6\text{Li}$ we get a maximum deceleration or acceleration of

$$a_{max} = \frac{\hbar k \gamma}{2m_{\text{Li}}} \approx 2 \cdot 10^6 \text{ m/s}^2 \approx 2 \cdot 10^5 \text{ g} .$$

3.2.2 Atom Magnetic-field Interaction

Now we will take a closer look at the effect of an external magnetic field \mathbf{B} on an atom. We start our calculations by adding an interaction term \hat{H}_{mag} to the undisturbed Hamiltonian

$$\hat{H} = \hat{H}_0 + \hat{H}_{LS} + \hat{H}_{MD} + \hat{H}_{mag} + \dots \quad (3.15)$$

where \hat{H}_0 is the central field Hamiltonian, \hat{H}_{LS} is the fine structure and \hat{H}_{MD} is the magnetic dipole interaction between the electron hull and the nucleus. We will assume the energy levels of the fine structure to be known and examine the hyperfine Hamiltonian.

$$\begin{aligned} \hat{H}_{HFS} &= \hat{H}_{MD} + \hat{H}_{mag} = -\mathbf{M}_I \cdot \hat{\mathbf{B}}_J - \mathbf{M}_J \cdot \hat{\mathbf{B}} - \mathbf{M}_I \cdot \hat{\mathbf{B}} \\ &= A \cdot \frac{\hat{\mathbf{I}} \cdot \hat{\mathbf{J}}}{\hbar^2} + \left(g_J \mu_B \frac{\hat{J}_z}{\hbar} - g_I \mu_N \frac{\hat{I}_z}{\hbar} \right) B \end{aligned} \quad (3.16)$$

with I and J indicating nucleus' or electron hull's magnetic moments \mathbf{M} respectively, $\hat{\mathbf{B}}_J$ being the magnetic field induced by the electron hull at the nucleus and the hyperfine coupling tensor A . In most cases it would be valid to assume $g_J \mu_B \gg g_I \mu_N$ and also for small B $A \gg g_I \mu_N B$ leaving us with what is called the **Zeeman effect of hyperfine structure**. Here we could neglect the nuclear magnetic moment and treat the external field as small perturbation to the field generated by the nucleus. Unfortunately the definition of "small" depends on the atom in question and can be

3.2 Interactions

state	A [MHz/ \hbar]	g_J	B_I [Gauss]
$2^2S_{1/2}$	152.136	2.002	86
$2^2P_{1/2}$	17.38	0.6668	30
$2^2P_{3/2}$	-1.15	1.335	1

Table 3.2: Field generated by the nucleus at the location of the (outer) electron for different states. The field decreases for states with angular momentum. For all states fields of the same or greater strength can be reached easily by external fields.

as low as a few gauss. To make a rough approximation where this regime starts we can rewrite the magnetic dipole interaction term as

$$A \cdot \frac{\hat{\mathbf{I}} \cdot \hat{\mathbf{J}}}{\hbar^2} = g_J \mu_B \frac{\hat{\mathbf{J}}}{\hbar} \cdot \hat{\mathbf{B}}_I .$$

This allows us to approximate the field $\hat{\mathbf{B}}_I$ generated by the nucleus at the location of the electrons

$$B_I \simeq \frac{A}{g_J \mu_B} .$$

Applying this formula to our ${}^6\text{Li}$ systems yields the results presented in table 3.2. It becomes apparent that the low field approximation will not hold in our case as we want to go as far as 1500 Gauss field strength.

We could also try to go to the other extreme and neglect the field generated by the nucleus and calculate the level splitting in the uncoupled $|JM_JIM_I\rangle$ basis. There is however a way to calculate the correct energy level shifts over the whole field strength regime. To do this we will have to diagonalize the whole hyperfine Hamiltonian 3.16 instead of assuming small perturbations. To do so we will first choose a basis. Since this calculation will become clearer with the uncoupled $|JM_JIM_I\rangle$ basis we will use it. Let us take a look at the complete hyperfine Hamiltonian for the $2s^2S_{1/2}$ ground state of ${}^6\text{Li}$. Since the nuclear spin of ${}^6\text{Li}$ is $I = 1$ we get six different states $|M_JM_I\rangle$. The calculation of the actual Hamiltonian requires some steps (refer to [Her08]) that would exceed the scope of this work so we will skip

forward to the finished Hamiltonian:

$$\hat{H}_{HFS} = \left(\begin{array}{c|cccccc} JI/M_J M_I & \frac{1}{2}1 & \frac{1}{2}0 & -\frac{1}{2}1 & \frac{1}{2}-1 & -\frac{1}{2}0 & -\frac{1}{2}-1 \\ \hline \frac{1}{2}1 & \frac{A}{2} + \mu_- B & 0 & 0 & 0 & 0 & 0 \\ \frac{1}{2}0 & 0 & \mu_B B & \frac{A}{2}\sqrt{2} & 0 & 0 & 0 \\ -\frac{1}{2}1 & 0 & \frac{A}{2}\sqrt{2} & -\frac{A}{2} - \mu_+ B & 0 & 0 & 0 \\ \frac{1}{2}-1 & 0 & 0 & 0 & -\frac{A}{2} + \mu_+ B & \frac{A}{2}\sqrt{2} & 0 \\ -\frac{1}{2}0 & 0 & 0 & 0 & \frac{A}{2}\sqrt{2} & -\mu_B B & 0 \\ -\frac{1}{2}-1 & 0 & 0 & 0 & 0 & 0 & \frac{A}{2} - \mu_- B \end{array} \right)$$

with

$$\mu_{\pm} = \mu_B \pm \mu' = \mu_B \pm \frac{\mu_N g_I}{g_J}$$

To obtain the evolution of the energy shifts we have to solve

$$\det(\hat{H}_{HFS} - W) = 0$$

Since this is a simple linear equation system it can be solved easily and yields (see also figure 3.4):

$$W_{\frac{1}{2}1} = \frac{1}{2}A + B\mu_- \quad (3.17)$$

$$W_{-\frac{1}{2}-1} = \frac{1}{2}A - B\mu_- \quad (3.18)$$

$$W_{\frac{1}{2}0} = \frac{1}{4}(2B\mu' - A - \sqrt{9A^2 - 4AB(\mu_+ + \mu') + 4B^2(\mu_+ + \mu')^2}) \quad (3.19)$$

$$W_{\frac{1}{2}-1} = \frac{1}{4}(2B\mu' - A + \sqrt{9A^2 - 4AB(\mu_+ + \mu') + 4B^2(\mu_+ + \mu')^2}) \quad (3.20)$$

$$W_{-\frac{1}{2}0} = \frac{1}{4}(-2B\mu' - A - \sqrt{9A^2 + 4AB(\mu_+ + \mu') + 4B^2(\mu_+ + \mu')^2}) \quad (3.21)$$

$$W_{-\frac{1}{2}-1} = \frac{1}{4}(-2B\mu' - A + \sqrt{9A^2 + 4AB(\mu_+ + \mu') + 4B^2(\mu_+ + \mu')^2}) \quad (3.22)$$

As summary we now know how the energy levels of the ${}^6\text{Li}$ system shift when in a magnetic field of moderate strength.

3.3 Laser Cooling

In this chapter we will discuss the application of chapter 3.2.1 and chapter 3.2.2 to build a trapping and cooling setup. First we will start with a slowing device that

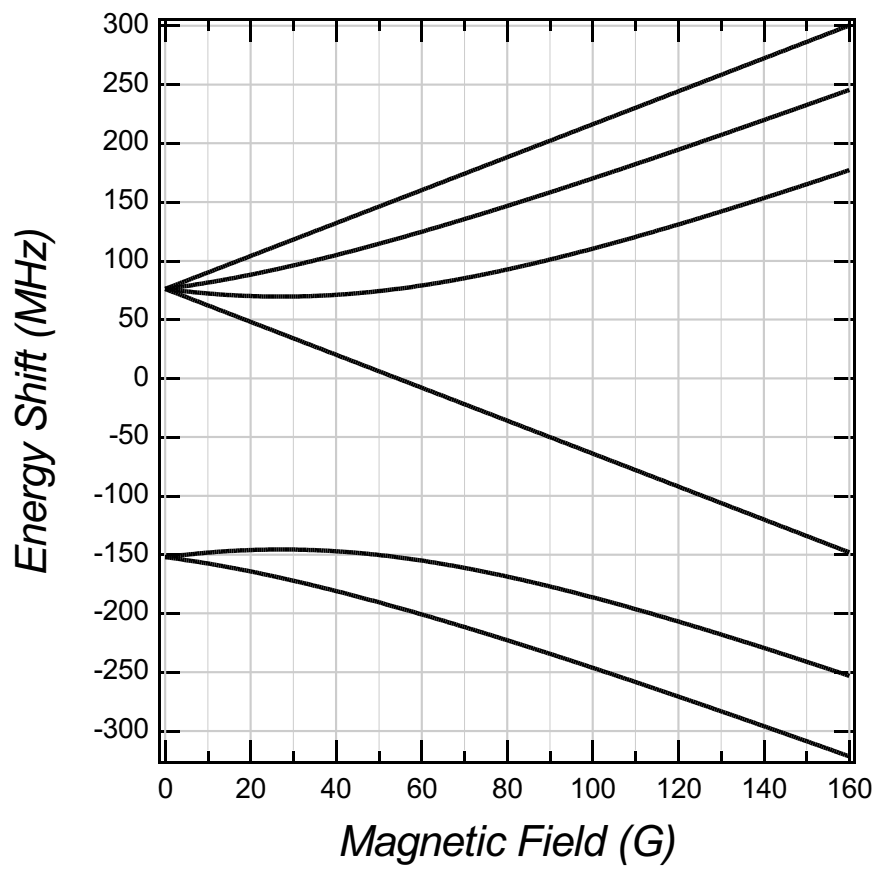


Figure 3.4: Zeeman shifts of the ${}^6\text{Li}$ ground state for moderate magnetic fields.

slows the atoms from thermal velocities to captureable ones. Then we will expand this to an actual trap that can hold atoms for long times.

3.3.1 Zeeman slower

As we learned in chapter 3.1.1 the atoms have a Boltzmann velocity distribution around $\bar{v} \approx 1500\text{m/s}$. As we will see in chapter 3.3.2 we need to slow them down to about 50 m/s to capture them. To do so we will use the spontaneous force we discussed in chapter 3.2.1.

There is however an important fact we have not taken into account yet. Due to the **Doppler effect** atoms moving towards the source of light see a frequency higher than the one we see in the resting frame. We can take it into account by defining an additional detuning

$$\delta_{\text{Doppler}} = kv = \frac{v}{c}\omega \approx 2\pi \cdot 1.49 \frac{\text{MHz}}{\text{m/s}} . \quad (3.23)$$

To get a feeling for the order of magnitude of this effect let us assume we slowed down our atomic beam by 100 m/s, the detuning changes by

$$\delta_{\text{Doppler}} = \omega_0 \frac{100 \text{ m/s}}{c} \approx 2\pi \cdot 149 \text{ MHz} \approx 25\gamma .$$

Looking back at figure 3.3 we see that we effectively lost the slowing force. Knowing that we need to cover a much larger velocity range than a few m/s it becomes apparent that we need to compensate for the Doppler effect. Luckily we have the solution already at hand as we discussed it in chapter 3.2.2. Using the Zeeman effect we can spatially tune the energy levels of the atom and thereby the resonance frequency. By applying the correct magnetic field we can exactly compensate the Doppler effect such that atoms stay in resonance throughout the slowing process. The slowing device described here is therefore called **Zeeman slower** and is derived from [Mol97].

To understand the dependence of the resonance frequency ω_0 on the magnetic field B for our ${}^6\text{Li}$ system let us take a look at our main cooling transition which goes from the $|{}^2S_{1/2}F = 3/2\rangle$ to the $|{}^2P_{3/2}F = 5/2\rangle$ state (a more detailed discussion of the ${}^6\text{Li}$ spectrum will follow in chapter 4.3.1). If we use the formulas we derived in chapter 3.2.2 we can calculate how the transition frequency scales with the magnetic field. To keep things simple we will (for now) limit us to the high field regime where the Zeeman shift is

$$\Delta E^{HFS} = \frac{\mu_B}{\hbar}(g_J m_J + g_I m_I)B .$$

3.3 Laser Cooling

This means that our transition frequency ω_0 will be shifted by an additional term

$$\begin{aligned}\delta_{mag} &= \frac{\Delta E_e - \Delta E_g}{\hbar} \\ &= \frac{\mu_B B}{\hbar} (g_{J_e} m_{J_e} - g_{J_g} m_{J_g}) + g_I (m_{I_e} - m_{I_g}) \\ &\approx \frac{\mu_B B}{\hbar} \text{ for } {}^6\text{Li} .\end{aligned}\tag{3.24}$$

If we plug in the constants for the ${}^6\text{Li}$ system we get

$$\frac{\delta_{mag}}{B} = 2\pi \cdot 1.4 \frac{\text{MHz}}{\text{G}} \approx 0.24 \frac{\gamma}{\text{G}} .$$

This means that we need about one Gauss magnetic field to compensate a velocity change of one m/s velocity.

Combining the two effects leads to an effective detuning

$$\delta_{\text{eff}} = \delta_0 + \delta_{\text{Doppler}} + \delta_{\text{mag}} = \delta_0 + \frac{v}{c}\omega - \frac{\mu_B B}{\hbar} .\tag{3.25}$$

To maximize the slowing force we have to keep δ_{eff} as close to zero as possible.

Therefore we need to find the correct spatial dependence of the magnetic field. Let us assume the atoms were somehow always resonant with the light. This would lead to a constant force and therefore constant deceleration a of the atoms. The formulas of uniform acceleration tell us that the atoms' velocity along their way is

$$v^2(z) = v_{\text{initial}}^2 - 2az$$

The discussed Doppler effect states that $\delta_{\text{eff}} \propto v(z) \propto B(z)$ therefore we can conclude that the magnetic field should look like this:

$$B(z) = B_0 \sqrt{1 - z/z_0}\tag{3.26}$$

where $z_0 = m_{\text{Li}} v_0^2 / \hbar k \gamma$ is the length of the magnet, $B_0 = \hbar k v_0 / \mu_B$ is the magnetic field at the beginning of the slower and v_0 is the maximum slowable velocity.

With this information we will be able to design a Zeeman slower (see 4.3.3) that will allow us to produce an atomic beam of ${}^6\text{Li}$ that is slow enough to be captured by the atom trap.

3.3.2 Magneto Optical Trap

In the last chapter we used a simple one-directional force to slow the atomic beam. This force can theoretically slow atoms to (almost) zero velocity. The problem is that it will then start to push the atoms back into the direction of the source. What we need is a force that always pushes the atoms towards a certain point which will become the center of our trap. In addition a second, dissipative force should slow the atom's motion in general and thereby keep the atoms cold. So we need confinement of the atoms in real and momentum space at the same time.

Optical Molasses

Let us first examine the momentum space confinement. The solution to this problem are two counter propagating beams of light with the same frequency, intensity and polarization. If the lasers are tuned below the atomic resonance (red detuned) an atom moving in opposite direction will, due to the Doppler effect, see a beam closer to resonance whereas an atom moving along the beam will see an even further detuned beam. Therefore the atoms have a much higher probability to absorb light moving in the opposite direction than themselves (see figure 3.5).

Now lets put it into formulas. The overall force \mathbf{F}_{OM} is simply the sum of the spontaneous forces from the two beams: $\mathbf{F}_{OM} = \mathbf{F}_+ + \mathbf{F}_-$. Using Equation 3.14 and Equation 3.23 we can describe the forces:

$$\mathbf{F}_{\pm} = \pm \frac{\hbar \mathbf{k} \gamma}{2} \frac{s_0}{1 + s_0 + (2(\delta_0 \mp |\delta_{\text{Doppler}}|)/\gamma)^2}$$

Neglecting terms of order $(kv/\gamma)^4$ and higher the sum of the two forces can be expanded to:

$$\mathbf{F}_{OM} \cong \frac{8\hbar k^2 \delta_0 s_0 \mathbf{v}}{\gamma(1 + s_0 + (2\delta_0/\gamma)^2)^2} \equiv -\beta \mathbf{v} \quad (3.27)$$

Now we have a force that always counteracts the current velocity of the atom thus slowing any motion. The dampening coefficient β depends on the properties of the laser beam. See figure 3.6 for some examples. Since this combined force damps motion in a similar way as a viscous fluid it is called **optical molasses**.

Doppler Limit

If this force were the only influence on the atoms they would be cooled to zero velocity and thereby zero temperature. Since this is clearly unphysical we must have forgotten an important effect. In this case it is the discrete size of the momentum

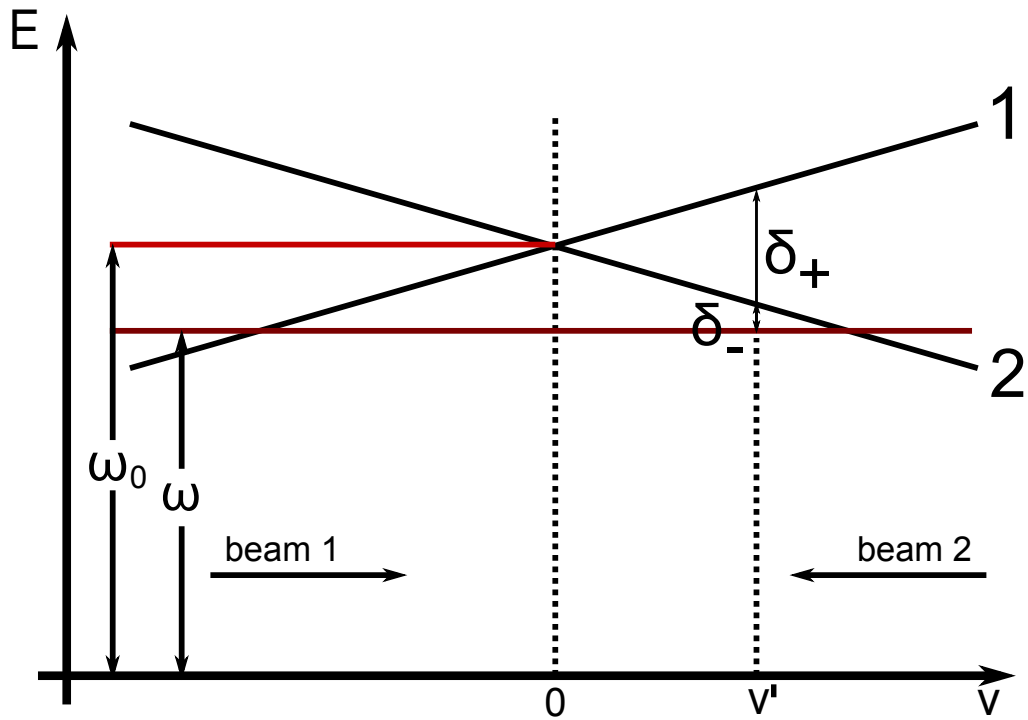


Figure 3.5: Concept of the optical molasses. The laser is tuned to a frequency $\omega < \omega_0$. Due to the Doppler effect the observed resonance frequency changes linearly with velocity v . Line 1/3 represents the shift for a atom moving in the same/opposite direction as the beam (positive/negative v). An atom with a velocity $v' > 0$ has a detuning δ_- with beam 2 δ_+ with beam 1. Since $\delta_- < \delta_+$ it absorbs more photons from beam 2 and is thereby slowed. In a real system beam 2 is just the retro-reflected beam 1.

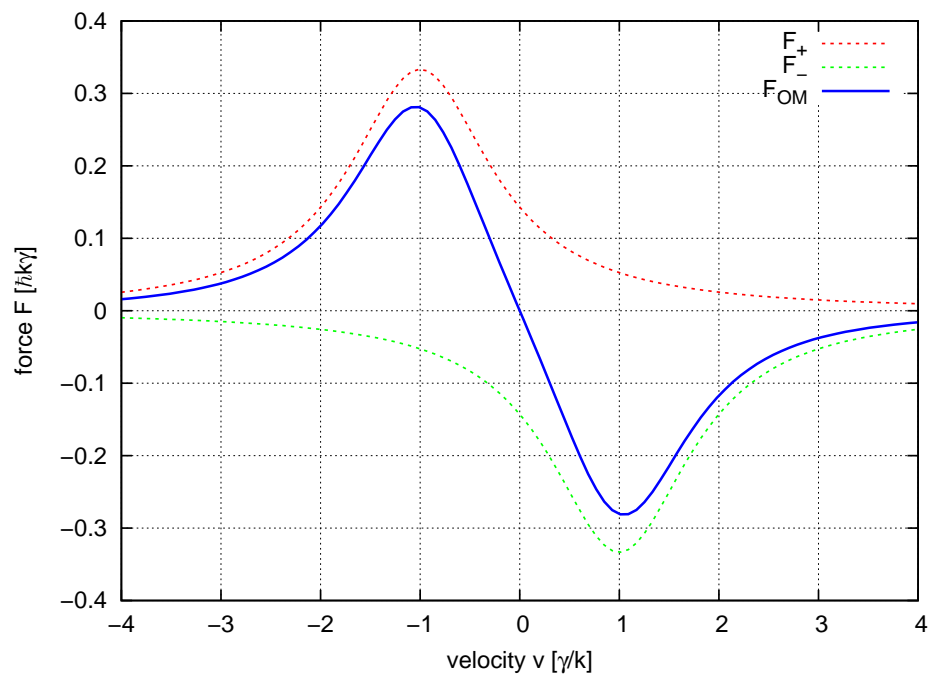


Figure 3.6: Force on the atoms in an optical molasses. For ${}^6\text{Li}$ the scales are $\gamma/k \approx 4$ m/s and $\hbar k \gamma / m_{\text{Li}} \approx 3.65 \cdot 10^6$ m/s²

3.3 Laser Cooling

steps. The atomic momentum changes in steps of $\hbar k$ per photon absorption. The temperature corresponding to the recoil of the photon emission is called **recoil limit**. For ${}^6\text{Li}$

$$T_{\text{recoil}} = 6 \mu\text{K} .$$

However this is not the limit for the optical molasses' temperature which is actually much higher. While the average of these momentum transfers is zero the root mean square scatter about zero is not. We can imagine the decays to cause a random walk in momentum space with the step size $\hbar k$ and step frequency $2\Gamma_{sc}$, where the factor of two accounts for the two beams. This random walk will result in diffusion of the atoms with a diffusion coefficient $D_0 = 2(\Delta p)^2/\Delta t = 4\Gamma_{sc}(\hbar k)^2$. Using the formulas of **Brownian motion** we can derive a minimal temperature

$$T_D = \frac{\hbar\gamma}{2k_B} \quad (3.28)$$

where k_B is the Boltzmann constant. This limit is reached for a very small saturation parameter $s_0/s \ll 1$ and detuning $\delta_0 = -\gamma/2$. Since this is the general limit for cooling techniques involving the Doppler effect it is called **Doppler limit**. It is a very general result since only the decay rate of the excited states enters as parameter. For our ${}^6\text{Li}$ system we get a limit of

$$T_{D,{}^6\text{Li}} = 140\mu\text{K} .$$

Spatial Confinement

Now we have the atoms confined in momentum space. Since the atoms can still slowly move out of the interaction region (diffusion), this alone will not be sufficient to build a good atom trap. To overcome this we will use the same trick we used in the Zeeman slower, namely applying a magnetic field. A linear magnetic field crossing zero creates a spatial dependence of the spontaneous force and also splits the energies of the Zeeman sublevels. Using two counter propagating circularly polarized laser beams will give rise to a spatial confinement while the optical molasses, realized by the same beams induces confinement in velocity space. The zero crossing of the magnetic field will then become the center of the trap. The details are explained in figure 3.7. Since this technique combines magnetic and optical forces to form a atom trap it is called **magneto-optical trap** (or in short MOT) [Met99].

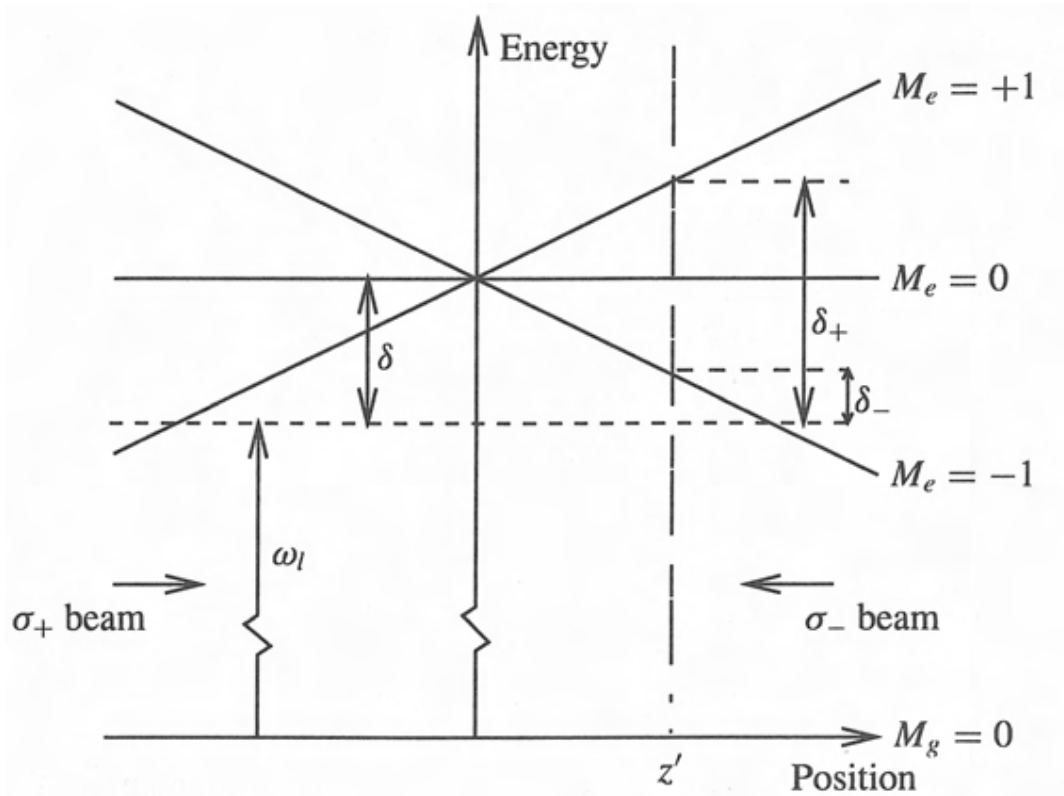


Figure 3.7: Principle of a MOT. The excited state $M_e = \pm 1$ is shifted up/down for $B \gtrsim 0$. The σ_{\pm} beam can drive $\Delta M = \pm 1$ transitions. The atom in position z' has a detuning δ_+ to the beam pushing it further out and δ_- to the beam pushing it back towards the center of the trap. Therefore more σ_- light is scattered and the atom is pushed back to the center. Here z is the quantization axis of the light. It depends on the orientation of the magnetic field. In real space the two light beams have the same polarization and are just seen differently.

Atom's Motion in the MOT

Now let's describe the motion of the atoms in a MOT in formulas. The total force on the atoms is given by

$$\mathbf{F}_{\pm} = \pm \frac{\hbar \mathbf{k} \gamma}{2} \frac{s_0}{1 + s_0 + (2\delta_{\pm}/\gamma)^2}$$

where the effective detuning δ_{\pm} is almost the same as we already defined for a single beam in 3.25

$$\delta_{\pm} = \delta_0 \mp \mathbf{k} \cdot \mathbf{v} \pm \mu_B B / \hbar .$$

Again for small Doppler and Zeeman shifts the denominator of the force can be expanded and we get the result:

$$\mathbf{F} = -\beta \mathbf{v} - \kappa \mathbf{r} \quad (3.29)$$

where the damping coefficient β is the same as defined in 3.27 and the spring constant

$$\kappa = \frac{\mu_B A}{\hbar k} \beta . \quad (3.30)$$

The force 3.29 leads to damped harmonic motion of the atoms. The damping rate is given by $\Gamma_{MOT} = \beta/m$ and the oscillation frequency $\omega_{MOT} = \sqrt{\kappa/m}$. For typical magnetic gradients $A \approx 10$ G/cm the oscillation frequency is on the order of kHz and is thus much smaller than the damping rate which is usually a few hundred kHz. Therefore the motion is overdamped with a characteristic restoring time to the center of the trap $2\Gamma_{MOT}/\omega_{MOT}^2 \approx$ milliseconds for typical values of the detuning and intensity of the laser.

The capture velocity v_c can only be obtained through numerical simulation since there are a lot of imperfections involved (magnetic field not $\propto \sqrt{z}$, beams have a non uniform intensity distribution and effects of the actual level scheme of the atoms). A typical value taken from [Met99] is $v_c \approx 50$ m/s.

Rate Equations

There are two very important properties of the MOT that are crucial for future experiments. First the loading rate L denoting the number of atoms we can capture per second. Since we will need a certain number of ${}^6\text{Li}$ atoms in the trap before we can perform further experiments this rate (if too low) could limit the whole experimental cycle. And second the lifetime of the MOT indicating perturbing effects due to the background gas that might limit future stages of the experiment (see chapter 5).

Obviously there has to be some kind of loss process that limits the total amount of atoms in the MOT or it would grow indefinitely. Another loss process will limit the total lifetime of the MOT when we stop capturing new atoms and just hold them.

- **One-body losses** are collisions of the trapped atoms with hot background gas. These collisions can transfer enough momentum onto the atom to expel it from the MOT. It can be minimized by reducing the background pressure for example by shutting off the atomic beam from the oven. The scaling of this effect is of the order $\mathcal{O}(n)$ with the atomic density.
- **Two-body losses** involve two atoms from the trap and a photon from the trapping beams to account for energy and momentum conservation.
 - In a **radiative escape** atoms in the ground and excited state attract each other due to their molecular potential $V_{SP} \propto r^{-3}$. Thereby they gain kinetic energy that they keep when the excited state decays and the attractive potential is lost.
 - In **state changing collisions** two atoms collide and change their spin state. The energy difference is converted to kinetic energy.

This accumulation of kinetic energy can cause the atoms to leave the trap. As two atoms are involved the effects scale with $\mathcal{O}(n^2)$.

With these scalings we can formulate a rate equation for the number of atoms in the MOT:

$$\frac{N}{t} = L - RN - \beta N^2 \quad (3.31)$$

with the loss rates R and β for one- and two-body losses.

4 Experiment

After discussing the principles of laser cooling we now turn to the real life system. In this chapter we will describe how we built the apparatus that actually implements the mentioned methods. We will start with the more technical part by describing the vacuum system. Then we will turn our attention towards the experiment control and how we regulate and measure the various parameters. After this we will finally take a look at our ${}^6\text{Li}$ system and its properties which we have to know to build the laser system. Having all tools at hand we can build the Zeeman slower and MOT.

4.1 Vacuum Chamber

Here we will give a short overview over the vacuum system as shown in figure 4.1. The main goal for the vacuum system was to achieve a ultra high vacuum in the range of 10^{-11} to 10^{-12} mbar while maintaining a good optical access for our experiments. This is needed to minimize collisions with the residual gas (see chapter 4.3.4). It was designed with a few important ideas in mind:

- **Simplicity:** Keeping all parts as simple as possible reduces the probability of errors and makes searching them much easier. This also means using commercially available parts whenever possible. In fact only the Zeeman slower and the re-entrant viewports were custom designed and built (see chapter 4.3.3).
- **Durability:** Once the machine is running it will be possible to run it for long times (years) without breaking the vacuum in the experimental chamber, even to refill the oven. To accomplish this the experimental and oven chamber are separated by a valve.
- **Flexibility:** Leaving room for changes around the experimental chamber.
- **Stability:** As it was clear at the time that the whole setup would be moved to another laboratory soon it was also built to be movable separate from the optical table it is mounted on.

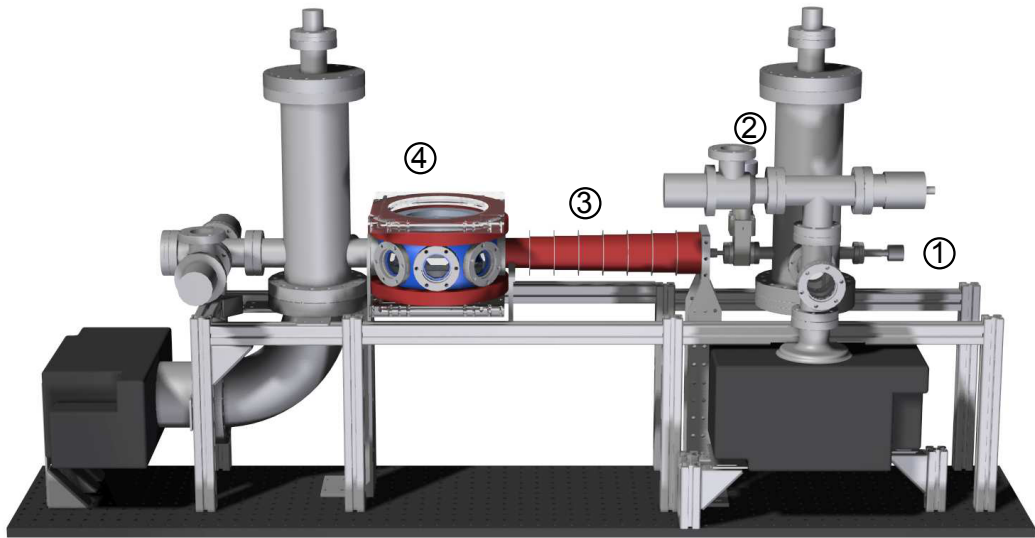


Figure 4.1: Vacuum system. Lithium atoms are evaporated in the oven (1) and travel towards the Zeeman slower. To avoid contamination of the gate valve (2) an aperture is placed in the vacuum. The flow can also be shut off by the oven shutter (not shown). After this the atoms are slowed along the Zeeman slower (3) and finally trapped in the center of the experimental chamber (4). Two ion pumps (black), two towers with Ti-sublimators (gray) and the NEG (Non Evaporable Getter) coating of the experimental chamber uphold the needed vacuum pressure.

The initial flux of atoms out of the oven of 10^{16} atoms/second is limited by the oven's nozzle. It allows about 0.3 % of the atoms to enter the first tower under a maximum angle of 12.5° . The geometry of the vacuum chamber allows for ≈ 0.1 % of these atoms to pass through the Zeeman slower which leaves us with a rate of $f_{\text{oven}} \approx 3 \cdot 10^{11} \frac{\text{atoms}}{\text{sec}}$. The other details of the vacuum system are described in [Rie10].

4.2 Experimental Control

In this chapter we will outline the system used to control the apparatus. For a relatively simple tasks such as loading a MOT the number of actions that have to be taken is small. But as the experiments grow more complex the control of the system can no longer be done by hand. Therefore we integrated a computerized control system right from the start. The main design goals were:

- **Flexibility** to add more components to the system as the apparatus grows in complexity without the need for a major redesign of the user interface or the underlying software. Also the system is not confined to one box but can be spread to wherever it is needed.
- **Robustness** against outside influence such as stray radio frequency noise or ground loops.
- **Speed** to cope with demanding applications such as feedback control systems with up to 1 MHz resolution or RF-switches with switching precision in the range of 50 ns.

It is very important that all actions are performed at exact times for each realization of the experiment. To meet these requirements we use a real-time system called LogicBox. The hardware was provided by the Physikalisches Institut of the Heidelberg University. Here it is guaranteed that the timings are met with precision in the order of 10 ns. To build a user interface we used LabView by National Instruments.

LogicBox

The core of each LogicBox is a field programmable gate array (short FPGA) which is basically programmable hardware. It also holds 4 extension slots where a number of different cards can be plugged in. In the current state of the setup we have a 32 channel digital I/O card in one box and a 16 channel digital to analog converter and a 16 channel analog to digital converter in another box. Each box is given a timing

array which basically holds the information which channel should have which value at any given time. This timing array is uploaded to the box via an USB connection. To ensure that all boxes have the same time base we use an external clock and trigger that are distributed to all boxes. While these boxes provide a flexible and extendable hardware setup it is good to be aware of the limitations of the various extension cards.

Current Limitations

For the digital channels the limiting factor is the decoupler. It provides a ground that is separate from the ground of the box itself. It limits the speed of each channel to about 30 MHz (which corresponds to a cycle time of 33 ns) and the high level to 4.2 Volts. For our purposes the speed is not critical since we usually operate in the milli or microsecond regime. Also the current the channels can drive is only a few mA. So the timing of the digital channels is more than fast enough while on the other hand current and voltage are good enough to drive TTL inputs but can be too low for other applications.

The bottleneck for the analog channels is the connection from the FPGA to the digital analog converter (DAC). The card holds two DACs with 8 channels each. Both of them are connected to the FPGA via a shared serial interface. This limits the update rate of each of the DAC's 8 channels. To change the value of one channel we need to transfer 24 bits of data. This can be done with a data rate of 10 MHz. To update all 16 channels on two DACs we therefore need about 50 μ s. The noise of the signal is within the specifications of the DAC used. It is about 1 mV on a 5 V signal

The DAC's counterpart the analog to digital converter (ADC) is connected in the same way and suffers the same shortcomings. It's accuracy is on the same level as the DAC's output. This means both DAC and ADC can be used for applications that do not need fast or very accurate signals.

For the scope of this work this hardware will be sufficient. In the near future we have some high speed DAC boards planned that can be used for more demanding applications.

LabView

Now that we have the hardware let's examine the software. It was entirely developed in LabView and serves two major purposes: First to provide an easy to use user interface to generate the mentioned timing arrays and to upload them to the LogicBoxes. Second to control and program the cameras used to take images of the experiment. To ensure maximum speed, responsiveness to user input and also flex-

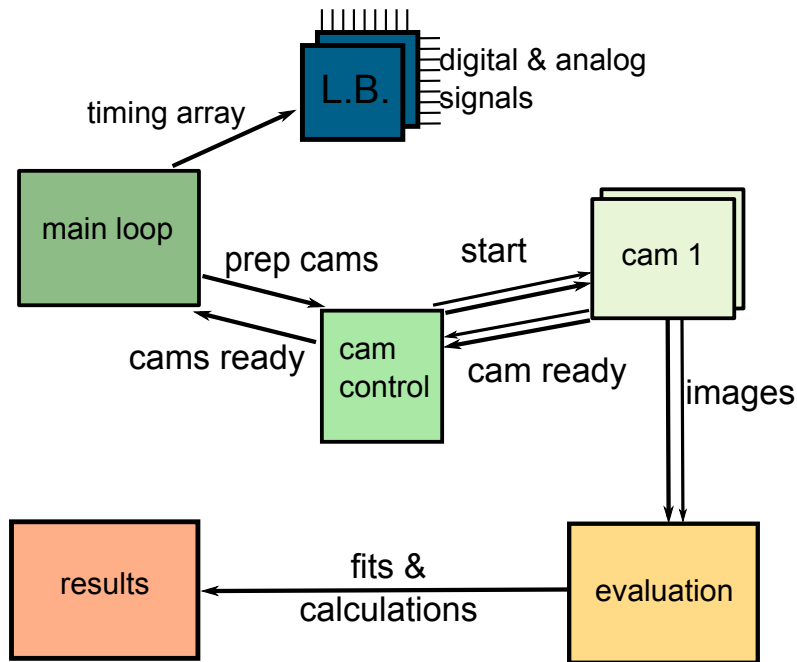


Figure 4.2: Overview of the LabView program structure. Separate loops connected via message queues acquire and evaluate data.

ibility in extending the software it is split into smaller subprograms (called loops) that run autonomously. These smaller parts communicate via globally managed lists (called queues). In figure 4.2 an overview over all parts is shown. To understand the general idea of the design we will follow the data path for one run. We will start with the main loop. This part takes the user input, calculates the timing arrays from it and uploads them to the LogicBoxes. It also tells the camera control loop to prepare the cameras for measurement. After that it waits for the cameras to signal that they are ready. The camera control loop waits for the main loop to tell it to prepare the cameras. On receiving the message it simply passes it to the camera loops (one for each camera). Each camera loop sets up its camera and starts an image acquisition, meaning that the camera will take an image after it receives a trigger from the LogicBox. It also signals the camera control loop that the camera is now ready. If all cameras are ready the main loop triggers the LogicBoxes. Which then start to process their timing arrays. At some point the cameras receive their trigger signals and take an image. The camera loops download the image to the computer and pass it along to the evaluation loop. This loop evaluates the images and calculates things like particle number or temperature. The results are passed to the results loop which

4.3 Cooling and Trapping

Property	Symbol	Value for D1	Value for D2
Wavelength	λ	670.992421 nm	670.977338 nm
Lifetime	τ	27.102 ns	
Natural Linewidth	γ	$2\pi \cdot 5.872$ MHz	
Saturation Intensity	I_0	7.59 mW/cm ²	2.54 mW/cm ²

Table 4.1: Properties of ⁶Li taken from [Geh03]

finally displays and saves the data. After one run the whole process begins anew.

At a first glance these interconnected loops seem to make the program unnecessarily complex. However they greatly enhance the overall speed and responsiveness of the system. For example the evaluation loop can already start to evaluate the image of camera 1 while camera loop 2 is still acquiring the image. Also the user interface is responsive while the experiment is still running as the main loop has nothing else to do.

4.3 Cooling and Trapping

Now that we have explored the underlying principles (in chapter 3) and the experimental tools (in chapter 4.1 and chapter 4.2) we can finally start to trap real atoms. In this chapter we will describe the cooling and trapping setup and present some properties. We will start out by describing the ⁶Li atoms with their distinct advantages and problems. Then we will prepare the laser system to provide the needed light and its control. Finally we will use all the above to build the Zeeman slower and the MOT.

4.3.1 ⁶Li System

Let us take a look at the relevant part of the ⁶Li level scheme (see figure 4.3). There are two transitions (called D1 and D2 for historical reasons) in the range of our laser (see 3.1.3). As we can see in table 4.1 their properties are almost the same except for the saturation intensity. Since a lower saturation intensity means that we need less laser power to effectively cool our atoms we will use the D2 line as cooling transition. We chose the $|2^2S_{1/2}F = 3/2\rangle$ to $|2^2P_{3/2}F = 5/2\rangle$ transition which is therefore called **cooler**. To understand the reason for these particular hyperfine levels we have to look at the different regimes of magnetic field strength separately.

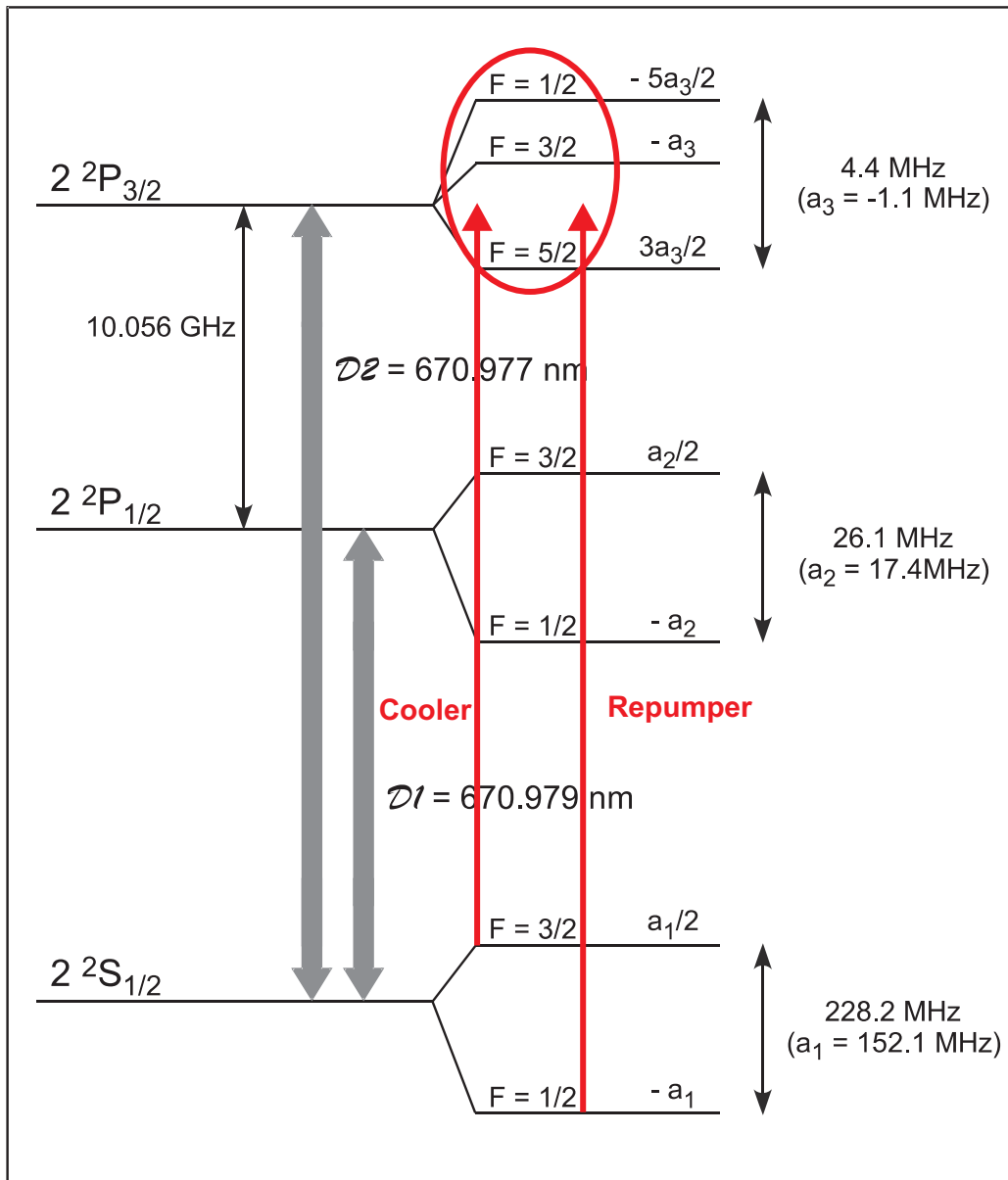


Figure 4.3: Lowest states of the ${}^6\text{Li}$ level scheme (spacing not to scale). Cooler and repumper shown without any detuning.

Low Field Regime

Let's turn our attention to the hyperfine levels for low or zero magnetic field. Here F is a good quantum number and the selection rules for dipole transitions are:

$$\begin{aligned}\sigma_{\pm}\text{-light: } \Delta m_F &= \pm 1 \\ \pi\text{-light: } \Delta m_F &= 0\end{aligned}$$

When we compare the splitting of the excited state ≈ 4.4 MHz with the natural linewidth $\gamma = 5.872$ MHz we see that the cooler is also relatively close to resonance with the other hyperfine states of $|2^2P_{3/2}\rangle$. If we always have perfectly polarized σ_+ light this is not a problem as it can only drive the transition with $\Delta F = +1$. However in our MOT we have magnetic fields that can change the quantization axis (see figure 3.7) so that σ_+ becomes σ_- light. Especially around the zero crossing of the magnetic field this leads to transitions into the $|2^2P_{3/2}F = 3/2 \text{ or } F = 1/2\rangle$ states. These states however have two possible decay channels, back into the $|2^2S_{1/2}F = 3/2\rangle$ state or into the $|2^2S_{1/2}F = 1/2\rangle$ state. Atoms in the $F = 1/2$ state are 228 MHz away from our cooling transition and therefore do not see the cooling beam anymore which means they are effectively lost. This state is called a dark state. To reintroduce these atoms into the cooling cycle a second laser frequency is needed. It is called the **repumper** and drives the $|2^2S_{1/2}F = 1/2\rangle$ to $|2^2P_{3/2}F = 3/2\rangle$ (or for the same reasons as before to $F = 1/2$) state. From there the atoms can decay back to the $|2^2S_{1/2}F = 3/2\rangle$ state and are thereby back in the main cooling cycle.

The actual power needed in each beam depends on the ratio with which atoms drop down to the $F = 1/2$ state and is roughly 2/3 cooler and 1/3 repumper for ^6Li . This is an unusually even power distribution for laser cooling. With other alkali atoms the strength of the repumper is of order 10^{-3} or less. In our experimental setup cooler and repumper will not be two independent beams but one beam containing two frequency components. How this is done is described in chapter 4.3.2.

High Field Regime

In the case of high magnetic fields things become a little easier. Using the results from chapter 3.2.2 we can calculate the scaling of the levels with the magnetic field. If we take a look at figure 4.4 we see that for high magnetic fields the excited state sublevels become four well separated states. Here F is no longer a good quantum number, instead we use the decoupled quantum numbers I and J . Using these we can formulate new selection rules:

$$\begin{aligned}\sigma_{\pm}\text{-light: } \Delta m_I &= \pm 1 \text{ and } \Delta m_J = 0 \\ \pi\text{-light: } \Delta m_J &= \pm 1 \text{ and } \Delta m_I = 0\end{aligned}$$

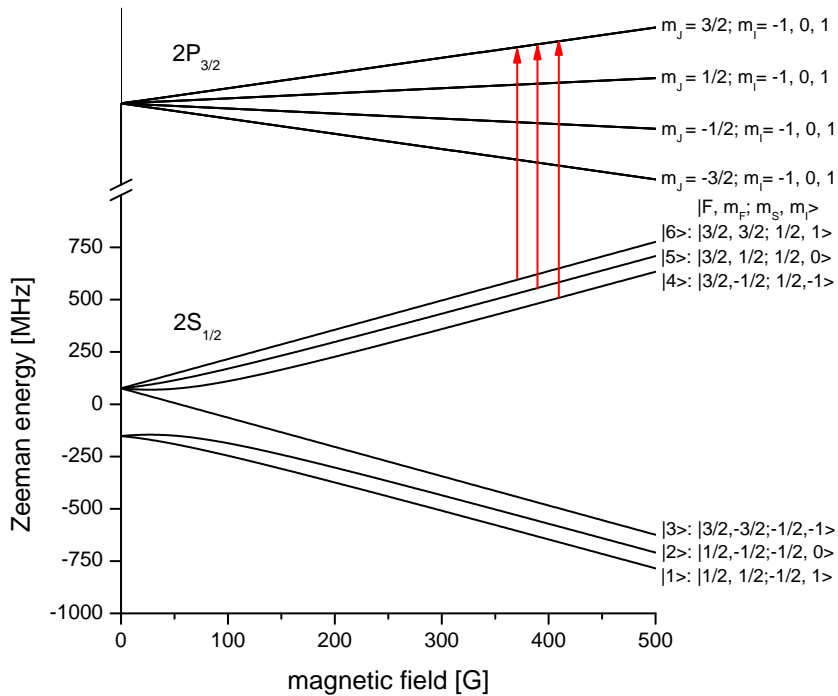


Figure 4.4: Scaling of the hyperfine levels at high magnetic field. Transitions in the wrong sublevel are now energetically impossible since the levels are several hundred MHz apart. There are three closed cooling transitions at our disposal so we can only cool 50% of the atoms in the high field regime.

With these we see that all possible transitions in figure 4.4 are closed. Therefore no repumper is needed.

Intermediate Field Regime

In between these two regimes the scaling of cooler and repumper is different. It is thus possible that the transition is not yet closed, but the repumper is already off resonance. This could lead to atoms that permanently fall down to the dark state and are lost. So if one wants to slow an atomic beam it is generally a good idea to avoid this regime.

4.3.2 Optical Setup

In this chapter we will discuss how we build the laser system meeting all the requirements that piled up so far. As a summary the laser system should have the following properties:

- **frequency:** is stable and tunable through a range of about 50 MHz to realize different values of the detuning δ_0 ,
- **power:** is tunable from about 0 to 30 mW per MOT beam to achieve saturation parameters s_0 from almost 0 up to 10,
- **stability:** in frequency and intensity to guarantee reproducible results over several thousand realizations,
- **ease of use:** so we can spend our time doing physics.

As discussed in chapter 3.1.3 we have an almost ideal source of light and the needed tools at hand. Now we will discuss how to use these to build our laser system. An overview of the whole system as it was built on the laser table is given in figure 4.5.

Beat Offset Lock

First we will discuss how to stabilize the laser's frequency and tune it in a controlled way. To measure the laser frequency we need a reference to compare it to. In this case this is the spectroscopy light that is provided by a separate laser setup. In this setup a similar diode laser is stabilized to the D2 line using a method called Pound-Drever-Hall laser frequency stabilization [Bla01] which in principle is Doppler free rf spectroscopy. We can assume this light to be on resonance to within a fraction of the natural linewidth. This light is then superimposed with light from the seed diode of the TA Pro laser on a photo diode. When the two lasers do not have exactly the same frequency a beating between the two will cause intensity fluctuations as the beams interfere constructive and destructive with the frequency $\omega_{\text{beat}} = \omega_{\text{TA}} - \omega_{\text{spect}}$. These fluctuations in brightness will be seen by the photodiode that converts the light to a electrical signal. Now we have to use some electronics to convert this AC beating signal to a DC signal that is proportional to the frequency ω_{beat} so we can feed it back to the laser control to tune the frequency accordingly. To do so we used commercial electronic components from MiniCircuits and put them together as shown in figure 4.6. To understand how the signal is processed we will follow it along the path:

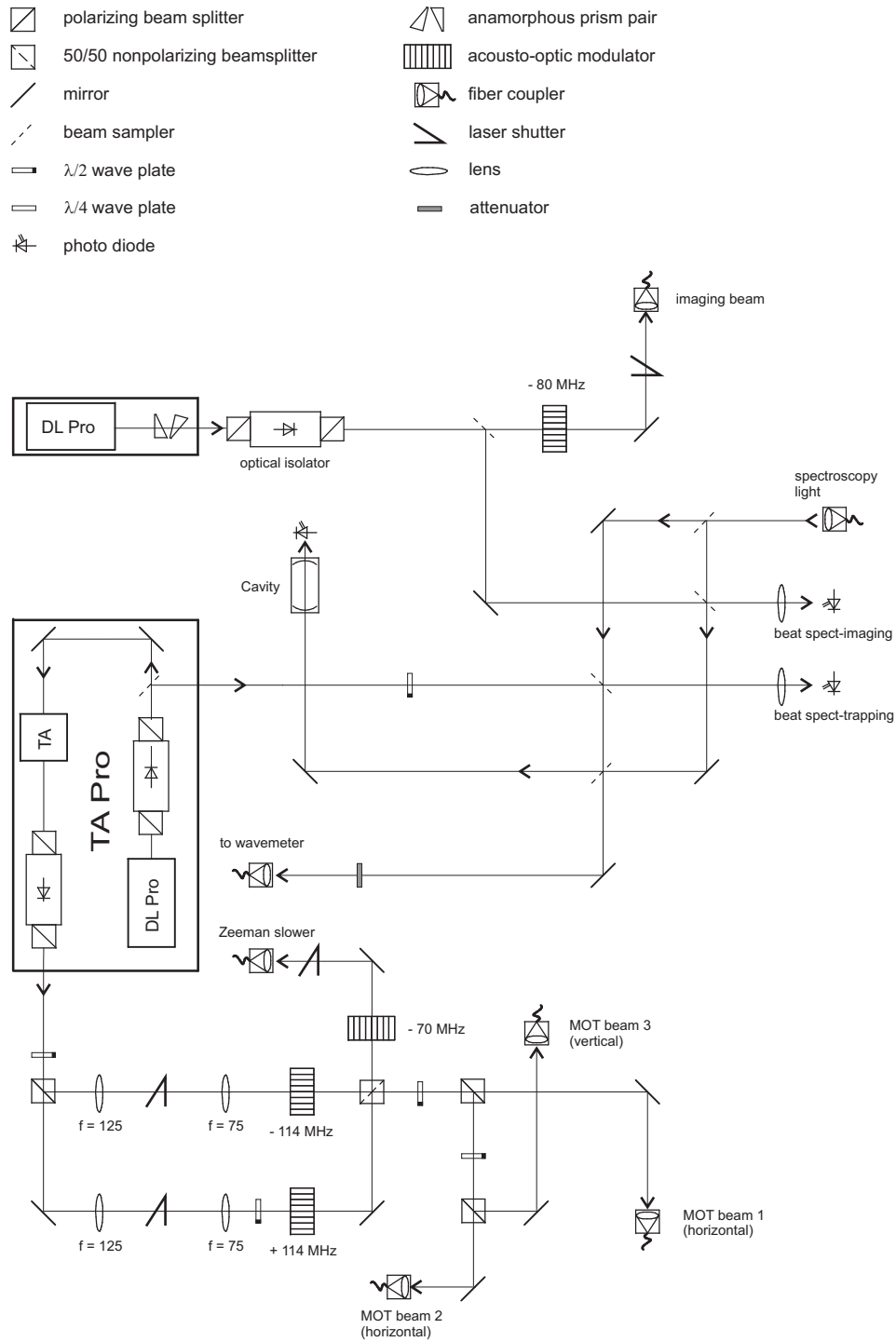


Figure 4.5: Optical system on the laser table.

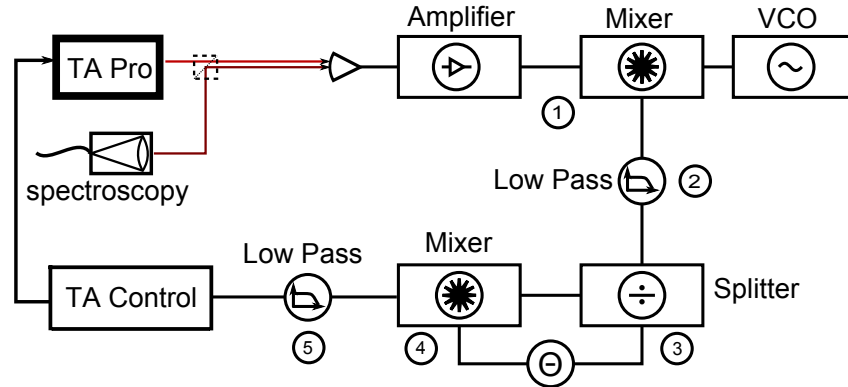


Figure 4.6: Schematic overview of the beat offset lock.

1. Mixer: Here ω_{beat} is mixed with another frequency ω_{VCO} . This signal is provided by an voltage controlled oscillator. This mixing will lead to new frequencies $\omega_{\text{beat}} \pm \omega_{\text{VCO}}$.
2. These are then fed through a low pass filter which only leaves $\omega_{\text{beat}} - \omega_{\text{VCO}}$.
3. The splitter sends the same signal along both paths. One is left unchanged whereas the other one is delayed through a cable of length l . This will lead to a extra phase $\Theta = (\omega_{\text{beat}} - \omega_{\text{VCO}})l/c_{\text{cable}}$
4. In the next mixer these two signals are again mixed together which leads to

$$U_{a \otimes b} \propto \cos(\omega_{\text{beat}} - \omega_{\text{VCO}} \pm (\omega_{\text{beat}} - \omega_{\text{VCO}} + \Theta))$$

5. In the last step the signal is again fed trough a low pass which only leaves us with the constant

$$U_{\text{final}} \propto \cos(\omega_{\text{beat}} - \omega_{\text{VCO}})l/c_{\text{cable}}$$

So at the end of the line we have an error signal that is related to the difference of the beatnote and the VCO frequency. This signal is fed to a PID controller that generates the control signal for the laser control electronics. By changing the voltage of the VCO we can therefore tune the detuning of the laser within the range of the used electronics (in this case approximately 100 MHz). Since we used a beatnote to lock the laser to a certain frequency this methods is referred to as **beat offset lock** as described in [Sch99].

MOT and Zeeman Slower

Now that we have a tunable, frequency locked laser we will use it to generate the needed laser beams for the Zeeman slower and the MOT. To accomplish this we lock our laser with $\omega_{\text{VCO}} \approx 80$ MHz red detuned from the cooler resonance. To generate the cooler and repumper part of the beams we split the outgoing beam in a 3 to 1 ratio between cooler and repumper (see lower part of figure 4.5). These beams are then shifted up and down (using AOMs discussed in chapter 3.1.3) by 114 MHz respectively. After the AOMs we have a cooler and a repumper beam detuned by 34 MHz from their respective resonance. After superimposing them again they are split into 4 beams for the Zeeman slower and the 3 MOT axis. The Zeeman Slower beam is shifted down by an extra 70 MHz so that it will have less effect on the atoms that are already trapped in the MOT (see chapter 4.3.4). All beams are then coupled into optical fibers that guide them to the vacuum chamber.

The polarization of all beams is still linear. To obtain the correct circular polarization for the MOT and Zeeman slower we integrated quarter wave plates into the beam outcouplers. The rest of the optics near the vacuum chamber can be seen in figure 4.7.

The output power of the laser is about 350 mW. After losing 10% in the AOMs due to the limited diffraction efficiency and losing another 50% due to imperfect coupling into the fibers about 80 mW in the Zeeman slower beam and 25 mW in each MOT beam remain.

Imaging

To provide a beam that can be tuned independently from the trapping and slowing beams we have a second laser in place. This DL Pro laser is locked to the same spectroscopy signal but here we used electronics that allow for a larger tuning range of approximately 1 GHz. This light can be used to take absorption images of the atom cloud. This technique will not be used in this work as simple fluorescence imaging will be enough for measuring the Zeeman slower and MOT.

On the chamber side we have placed two lenses to collect the light and focus it on a CCD camera. This very simple imaging setup is however good enough to measure simple properties like the atom number.

4.3.3 Zeeman slower

Now that we have a suitable vacuum chamber that provides us with a constant stream of fast ${}^6\text{Li}$ atoms and a laser to stop them we can build our Zeeman slower.

4.3 Cooling and Trapping

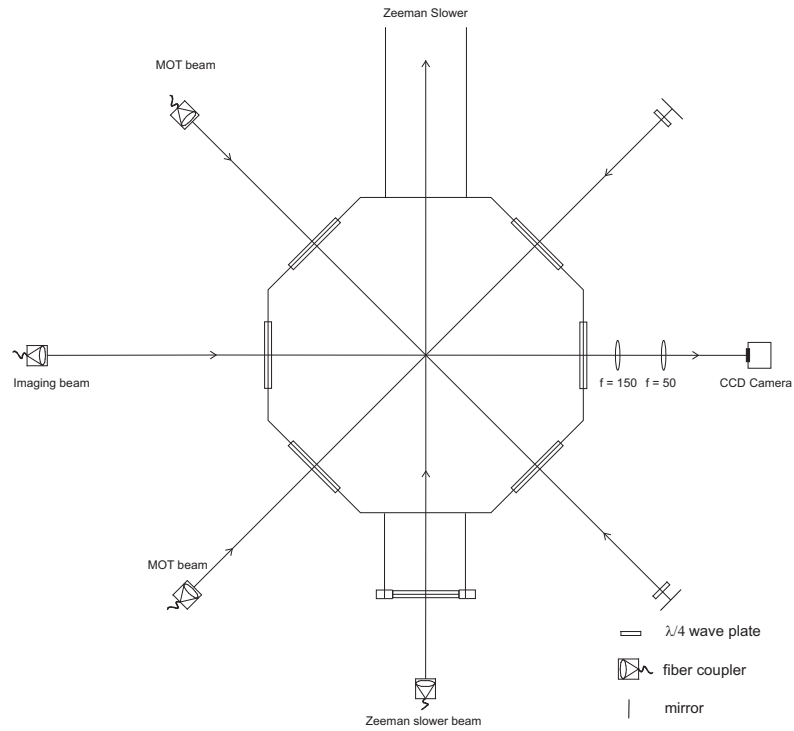


Figure 4.7: Optics setup around the experimental chamber. Each fiber coupler contains a collimation lens and a quarter wave plate to achieve the correct polarization. Both MOT beams shown here have σ_r polarization. As the projection onto the magnetic field defines if σ_r is seen as σ_{\pm} light and the field crosses zero at the center of the trap we end up exactly with the needed polarization. For the vertical beam (not shown here) the polarization is exactly opposite.

Possible Zeeman Slower Configurations

First we have to revisit the problem of finding the correct configuration of the magnetic field. As discussed in chapter 3.3.1 the slope of the field is $\propto \sqrt{z}$ however we could still add a offset field. Also we have to keep in mind that the Zeeman slower beam crosses with the MOT beams. It has to be detuned far enough to not disturb the trapping of the atoms. Assuming we can tune our laser to any given detuning there are generally three possible configurations:

1. An **increasing field** configuration where the highest magnetic field is near the end of the slower. This would have the advantage that the Zeeman slower beam would be very far detuned from the atoms that are already trapped in the atom trap. On the other hand high magnetic fields near the MOT would require compensation coils to make sure the slower field does not interfere with the MOT. Also high fields always mean heat which is very undesirable near the experimental chamber as it increases the background pressure.
2. A so called **spin-flip** configuration where the magnetic field crosses zero. This would require lower absolute fields thus producing less heat. The problem with this setup is that we spend more time in the range of intermediate field strengths where we have the risk, that atoms permanently drop into a dark state (see chapter 4.3.1). Because of this we decided in favor of
3. the **decreasing field** configuration. Here the Zeeman slower field can smoothly fade into the MOT field. In this way the MOT field is used to effectively enlarge the Zeeman slower. The offset is chosen such that the atoms are resonant with a beam detuned by

$$\delta \approx 125 \text{ MHz} \approx 16 \gamma$$

At this detuning we have a scattering rate with the atoms in the MOT of

$$\Gamma_{sc}(\delta = 125 \text{ MHz}, s_0 = 30) = 1.4 \cdot 10^{-2} \gamma$$

This will in fact push the center of the MOT towards the end of the Zeeman slower but it will not hamper the trapping of atoms much. In this setup we will be in the high field regime where the cooling transition is closed most of the time. For the remaining path at the end of the slower we also use a repumper beam.

Design of the Zeeman Slower

There are other parameters like the length or the outer radius that can dramatically affect the performance of the slower. Here we followed the proven technology of a previous design in our group [Ser07]. From there we also took the calculations for the magnetic field displayed in figure 4.10. A longer slower with even higher fields would allow for larger velocities to be slowed but would also decrease the solid angle towards the experimental chamber. This limits the maximum slowable velocity to about 700 m/s which is about 10% of the velocity distribution. Since the atoms leaving the oven have a 50% chance of being in either hyperfine level of the ground state we can only slow half of them. This leaves us with a maximum achievable flux of slow atoms at the end of the slower in the order of 10^{10} atoms/sec.

The only detail that was changed in the design is the cooling mechanism. Here we used the spacing between the vacuum tube and the coils to implement a water cooling (see figures 4.11, 4.12 and 4.9 for details). To accomplish this the slower tube had to be machined from one steel tube. In the middle we have a conic vacuum tube. On the oven side it has an opening of 5 mm diameter which opens to 12.2 mm at the other end. This allows the ^6Li atoms from the oven to pass through the tube without hitting the walls and on the other hand forms a differential pumping stage, protecting the vacuum pressure inside the experimental chamber as it separates it from the oven chamber where the pressure can be higher due to the hot oven.

Around the vacuum tube there are four channels for cooling water. These will cool the coils that sit on the outer casing. The coils are wound around the 36 mm diameter metal cylinder. There are 8 separate coils in total that are spaced 1 mm apart by metal rings. The coil nearest to the experimental chamber has a separate power supply to match the magnetic field with the MOT. Since the coils were wound without any thermal conducting paste or glue the bottleneck of the cooling setup is the heat transfer from the wire to the heat sink. In the normal use case this is not a limiting factor as the slower coils are only active for about one second (see 4.3.4) opposed to a cool down time of about 10 seconds where the slower is not needed. If we continuously use the slower coils they will heat up to about 150°C (at the far end, see figure 4.8) in about 30 minutes.

The light for the slower is shone in from the far end of the vacuum chamber (see figure 4.7 and figure 4.1). The focus of the fiber outcoupler is chosen such that the beam matches the opening angle of the conic vacuum tube of the slower and focuses inside the oven. To align this beam the oven shutter that is polished on both sides was used to reflect the beam out of one rear window. The power of the Zeeman slower light $I \approx 80\text{ mW}$ and therefore the absorption line is power broadened with $s_0 \approx 30$. This ensures full saturation of the cooling transition and helps to compensate for

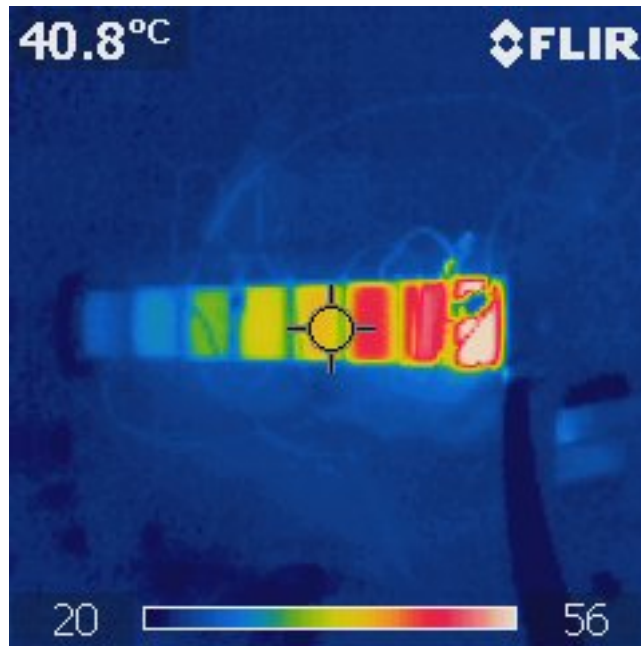


Figure 4.8: Infrared picture of the Zeeman slower when ran continuously for 10 minutes. The outer layers of the largest coils heat up while the small coils remain cool.

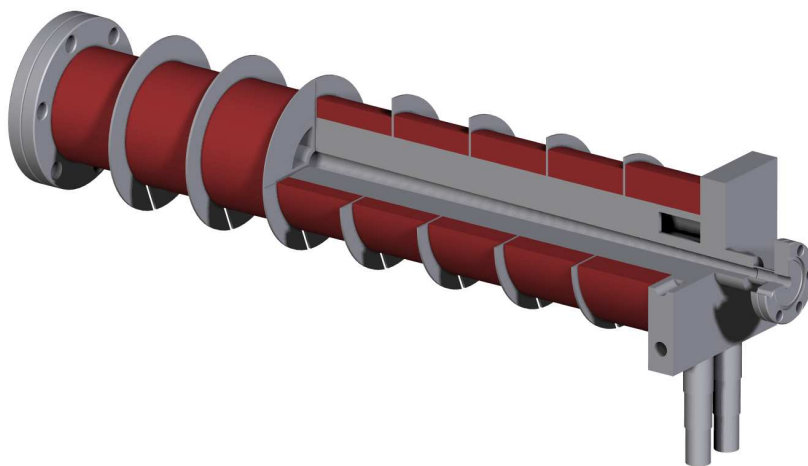


Figure 4.9: Zeeman slower with coils and cooling channels.

4.3 Cooling and Trapping

Property	Value
Current for coils 1-7	6.5 A
Current for coil 8	5.5 A
length	40 cm including MOT field
max. slowable v	≈ 700 m/s
maximum field	650 Gauss
expected flux	$\approx 10^{10}$ atoms/sec
detuning	-125 MHz
saturation parameter s/s_0	10
heat dissipation	300 W

Table 4.2: Properties of the Zeeman slower

small irregularities in the magnetic field.

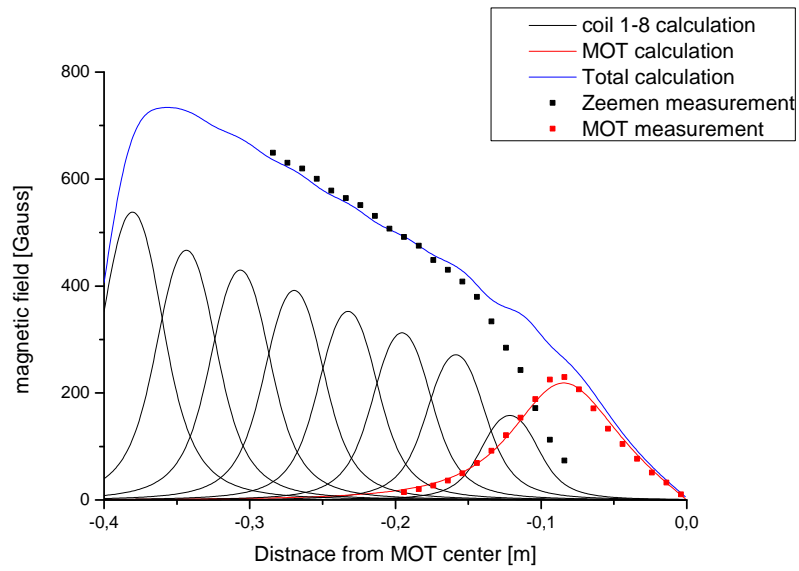


Figure 4.10: Measured and calculated fields of the Zeeman slower and MOT.

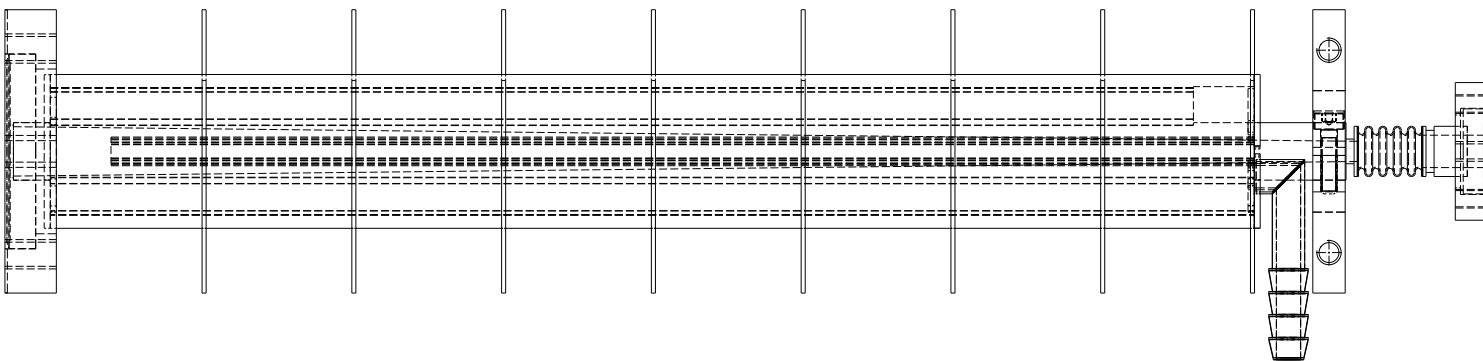


Figure 4.11: Front view of the Zeeman slower.

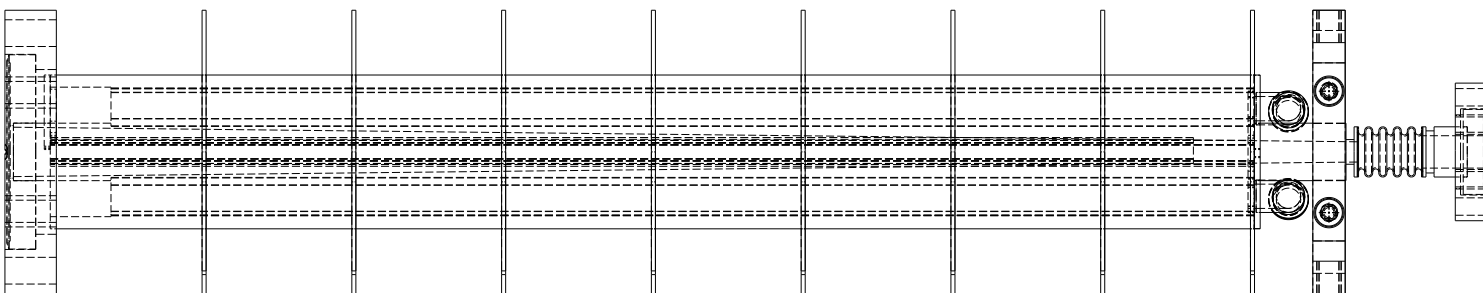


Figure 4.12: Top view of the Zeeman slower

Properties of the Slower

To quantify the effectiveness of the slowing process we measure the velocity profile of the atoms leaving the slower with the magnetic field turned on and off respectively. What we expect to see is a Boltzmann velocity distribution of the atoms in the direction of the beam and, with the Zeeman slower on, a distinct peak on the slow end of the distribution.

To measure this distribution we cross the imaging beam with the atomic beam under an angle of 45° . This way the light will have a certain momentum component along the path of the atoms and due to the Doppler effect only the atoms with velocity v_z will be resonant with the beam. By sweeping the detuning of the imaging laser δ_{image} through a certain range we can cover most of the Boltzmann distribution. With

$$\delta_{\text{image}} = -\frac{v}{c} = -\frac{v_z}{c} \cos 45^\circ$$

where the cosine is due to the fact that we shine in the light under an angle of 45° and the minus sign represents the blue detuning since we shine in the light from behind the atoms. With this formula we can relate detuning and velocity and get the results displayed in figure 4.13. Since we had to cover a unusually large range of detunings we operated the laser free-running and measured the frequency with a wave-meter. To minimize stray light we kept the beam diameter relatively small (≈ 2 mm). The intensity of the imaging beam was 6 mW. The fluorescence signal was recorded with the camera setup shown in figure 4.7. To get a strong enough signal exposure times of 2 seconds were necessary.

As a test of the measurement method we can fit a Boltzmann distribution to the data and check if the temperature matches that of the oven. Since the ground state of ${}^6\text{Li}$ is split in two hyperfine levels ($F = \frac{1}{2}, \frac{3}{2}$) that are both within range of the detuning sweep we have to add two Boltzmann distributions:

$$F(v_z) = A \left(\frac{m}{k_B T} \right)^{\frac{3}{2}} v_z^2 e^{-\frac{mv_z^2}{2k_B T}} + \frac{1}{2} A \left(\frac{m}{k_B T} \right)^{\frac{3}{2}} (v_z - v_0)^2 e^{-\frac{m(v_z - v_0)^2}{2k_B T}} - B \quad (4.1)$$

where k_B is the Boltzmann constant, m the mass of ${}^6\text{Li}$, T the temperature, A a scaling factor and B the offset due to background light. The first term represents to the upper hyperfine state $F = \frac{3}{2}$. The second term is shifted by the velocity $v_0 = 153$ m/s that corresponds to the splitting of the two levels of 228 MHz. Also it is weighted by the ratio of the degeneracies of the two states which is $\frac{g_{1/2}}{g_{3/2}} = \frac{1}{2}$. Fitting this function to the data yields the results displayed in table 4.3.

The temperature obtained from the fit is about 50 K higher than the actual oven temperature of 400°C . This indicates either an systematical error in the imaging

4.3 Cooling and Trapping

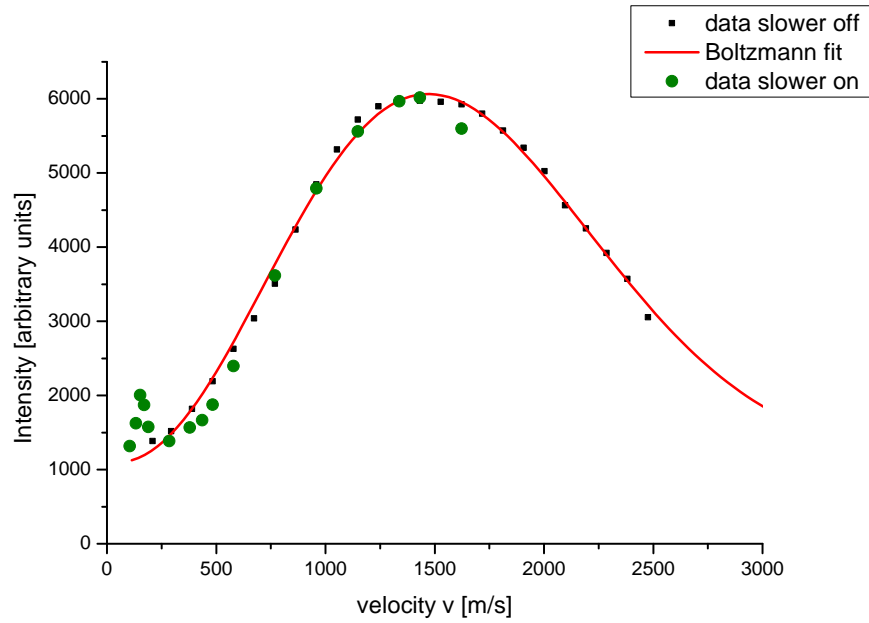


Figure 4.13: Without the magnetic field and the slower beam we get a Boltzmann distribution with $T = 728$ K. With the Zeeman slower operational we get a distinct peak at the slow end of the velocity distribution and depletion (but not a cut-off) of velocities ≤ 700 m/s. These were slowed by the slower into the peak.

Parameter	Value	Error
A	4557 [a.u.]	60 [a.u.]
B	-1062 [a.u.]	46 [a.u.]
T	728 [K]	7 [K]

Table 4.3: Fit results for the unslowed beam.

setup or we neglected an effect that influences the distribution in some way. The results are however good enough to make some qualitative statements.

In this fit we assumed that all atoms produce the same fluorescence signal when in resonance. This is not a priori evident because slow atoms need more time to cross the interaction region and should therefore scatter more light. However, an atom with $F = \frac{3}{2}$ has a approximately 15% probability to drop into the (dark) $F = \frac{1}{2}$ state with each absorption. Thereby an atom can no longer be seen after a mean of 6 to 7 scattered photons. With an interaction region of about 2 mm length even fast atoms with $v = 1000$ m/s could scatter 12 photons (assuming full saturation) and have therefore a high probability to be pumped into the dark state.

In the next step we turned on the Zeeman slower beam and the magnetic coils. The MOT coils were left off since we wanted to measure the atoms with no magnetic field. Therefore the last quarter of the Zeeman slower is not operational and the atoms were not slowed down to the capture velocity of the MOT. Instead the slow atoms have a speed of about 150 m/s. However we can see a depletion of the velocities $v_z \leq 700$ m/s. There is no clear cut-off since it is overlaid by the $F = \frac{1}{2}$ atoms that are unaffected by the slower. Also the height of the peak seems to small considering the results of chapter 4.3.4.

The most important test for the Zeeman slower is however the loading rate of the MOT. As we will see in the next chapter it is already very good with the current settings of the Zeeman slower. Therefore we did not optimize the Zeeman slower further.

4.3.4 MOT

Now we have to take the final step of trapping the now slow atoms. In this chapter we will discuss how we build the MOT and present its most important properties.

Setting up the MOT

With the bare vacuum chamber in place the two MOT coils were placed above and below the vacuum chamber (see figure 4.14). These produce a magnetic quadrupole field that will provide an almost linear magnetic field gradient around the center of the chamber. It is important to match the zero of the magnetic field with the center of the MOT beams to maximize the size of the MOT. The coils are therefore built to fit the vacuum flanges exactly, allowing almost no room for displacement.

In the next step the MOT beams were aligned to cross each other in the center of the chamber as shown in figure 4.15. This resulted in a first realization of the MOT which was subsequently fine tuned by maximizing the fluorescence of the

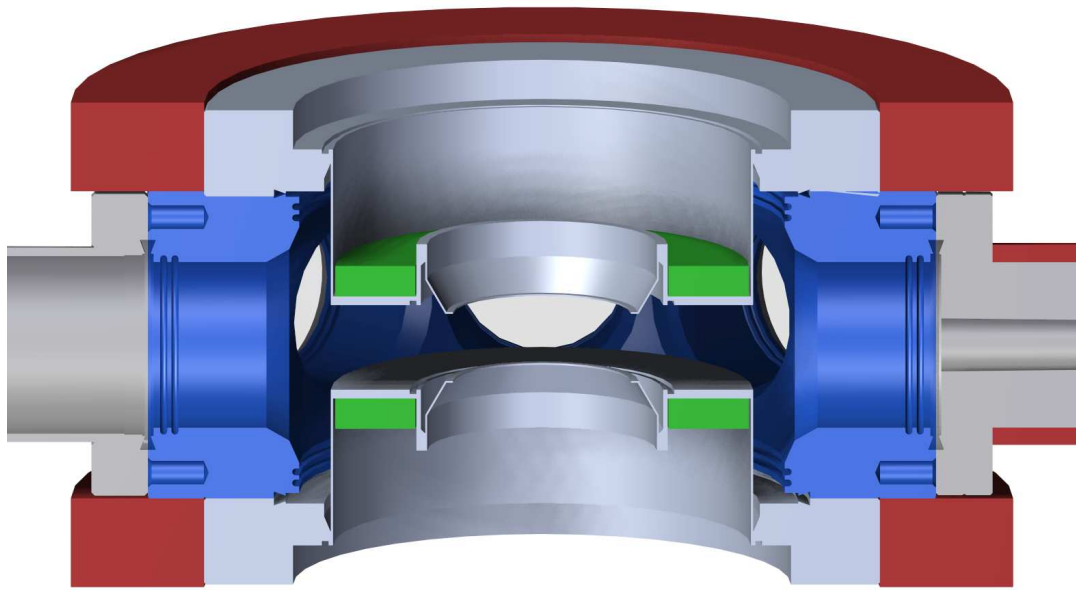


Figure 4.14: Schematic of the experimental chamber. The MOT coils are pictured in red while the vacuum flange is gray. Both are mounted on top and below the octagon (blue). Shown in green are (not yet installed) coils to produce even stronger magnetic fields than the MOT coils to tune the scattering length. On the right side is the exit aperture of the Zeeman slower. The MOT beams have a diameter of about 15 mm to barely fit between the two reentrant viewports.

atom cloud.

Imaging the MOT

One realization of the MOT can be seen in figure 4.16. While the MOT can be seen by the naked eye, we need an imaging system that has well known properties to make quantitative measurements. To observe the MOT a simple setup of two lenses and a CCD camera (as shown in figure 4.7) is good enough. From the image this camera takes we can calculate the number of atoms in the trap making following assumptions:

- The CCD chip has a linear response to the number of photons that hit a certain pixel. This is true as long as the chip doesn't saturate in any pixel.
- The photons emitted by the atoms are not reabsorbed by another atom of the cloud.
- The scattering rate of photons is constant.

If these assumptions are not fully met (for example photons can be reabsorbed in large MOTs) we can still get a lower limit for the atom number.

Knowing the solid angle Ω we cover with our image and the properties of our camera we can calculate the number of atoms in the MOT.

$$\Omega = \frac{r_{aperture}^2 \pi}{4\pi d_{lens}^2} \approx 0.0021 \quad (4.2)$$

This is the fraction of photons the camera captures. To go on we need to understand the internals of the camera a little bit better. The incident light is focused onto a CCD chip. This chip converts photons to electrical charge. This charge is then read out and converted to a digital value. What we need to know is the conversion factor η of photons to digital counts. This calibration can be done by shining a defined number of photons onto the chip. We can get this defined number by shining a laser of defined power onto the camera for a well known time. Using a $4.5 \mu\text{W}$ beam for $t = 31 \mu\text{s}$ we get:

$$\eta_{photons} \approx 1.22 \frac{\text{photons}}{\text{count}}$$

That means the number of photons actually emitted from the cloud is

$$N_{photons} = \eta N_{counts} \Omega$$

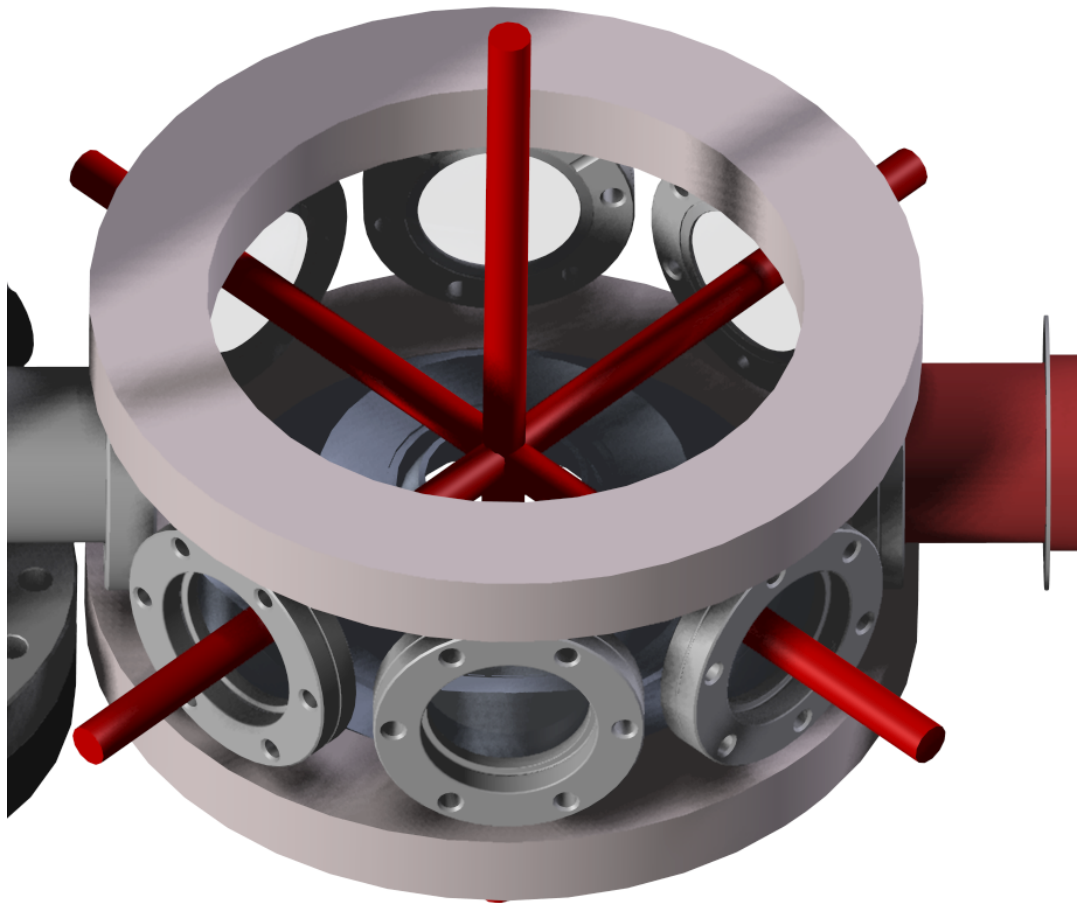


Figure 4.15: Schematic overview of the beam placement of the MOT beams. The vacuum chamber itself and the upper reentrant viewport are not shown for better visibility.

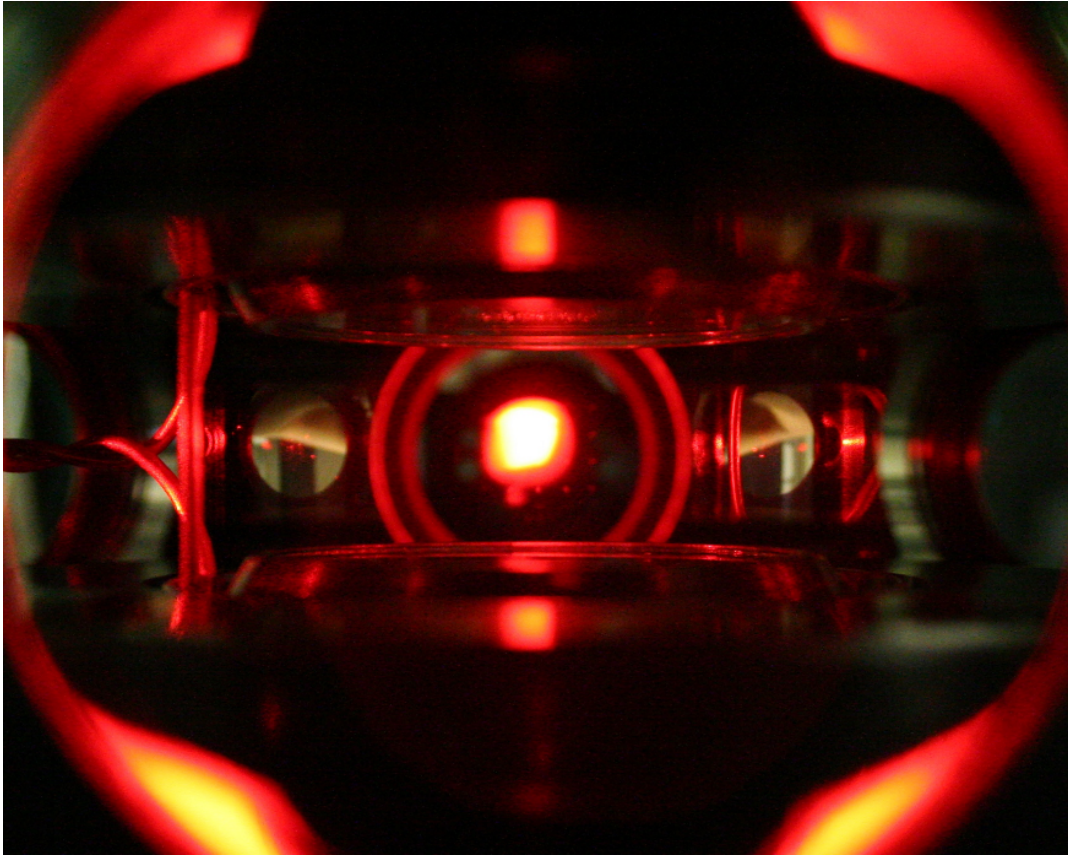


Figure 4.16: Cloud of ${}^6\text{Li}$ atoms held by the MOT. The red dot that sits in the center of the vacuum chamber is the atom cloud. It is visible since atom in the excited state emit the light in all directions with Γ_{sc} per atom. The box like shape is due to the limited size of the MOT beams.

4.3 Cooling and Trapping

which can be converted to an atom number using Γ_{sc}

$$N_{atoms} = \frac{\eta N_{counts}}{\Gamma_{sc} \Omega} \quad (4.3)$$

Here N_{counts} is the sum of counts over the whole chip. It is important to note that through Γ_{sc} the detuning δ and the saturation parameter s_0 enter the formula. We can however assume the scattering rate to be in its maximum of $\Gamma_{sc} = \gamma/2$ to get a lower limit for the atom number.

Loading the MOT

With a diagnosis tool at hand we can characterize the MOT in more detail. First we will measure the loading rate. Solving Equation 3.31 in the high density regime where we can neglect one-body losses yields:

$$N_{load}^{high\ n}(t) = \frac{L}{\beta n_0} (1 - e^{-\beta n_0 t})$$

where n_0 is the saturation density. For a typical oven temperature of $T = 350^\circ\text{C}$ the measurements yield a loading rate of

$$L = 3 \cdot 10^8 \frac{\text{atoms}}{\text{sec}} \quad (4.4)$$

which results in a maximum number of atoms in the MOT of:

$$N_{max}^{350^\circ\text{C}} = 1.2 \cdot 10^9 \text{ atoms} \quad (4.5)$$

A typical experimental cycle will only need 10^8 atoms in the MOT allowing for short loading times of about one second.

Lifetime in the MOT

Besides the loading rate the lifetime of the MOT is a very important parameter because it indicates the level of background collisions. We can measure it by holding a small number of atoms without loading new ones. With n small we can neglect the two-body losses and Equation 3.31 can be solved easily:

$$N_{decay}^{low\ n}(t) = N_0 e^{-Rt} \quad .$$

To measure these rates we record the fluorescence signal over a period of time. The time we can take to measure is limited by the heating of the MOT coils and the

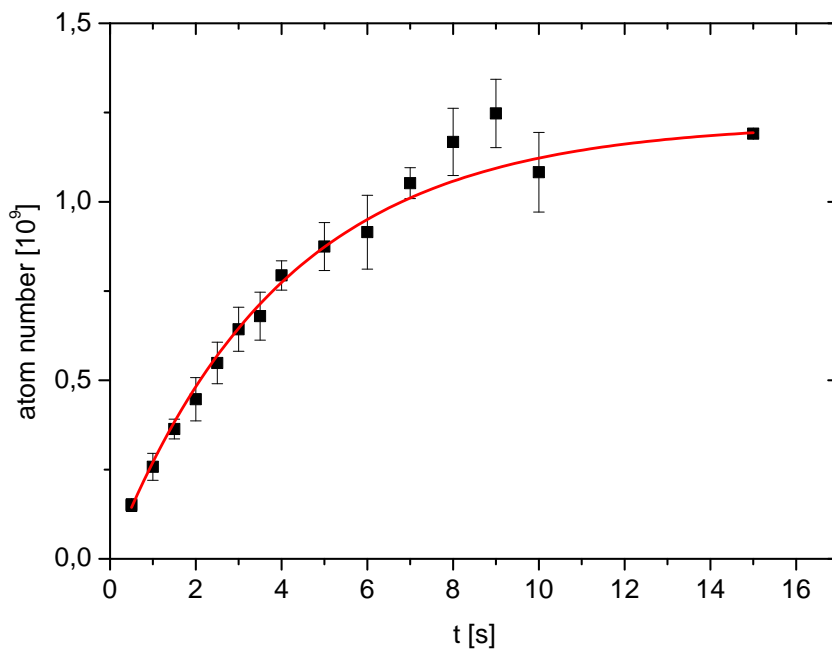


Figure 4.17: Number of trapped atoms in the MOT with oven temperature $T = 350\text{ }^{\circ}\text{C}$. Error bars represent the variation over 3 loading cycles.

4.3 Cooling and Trapping

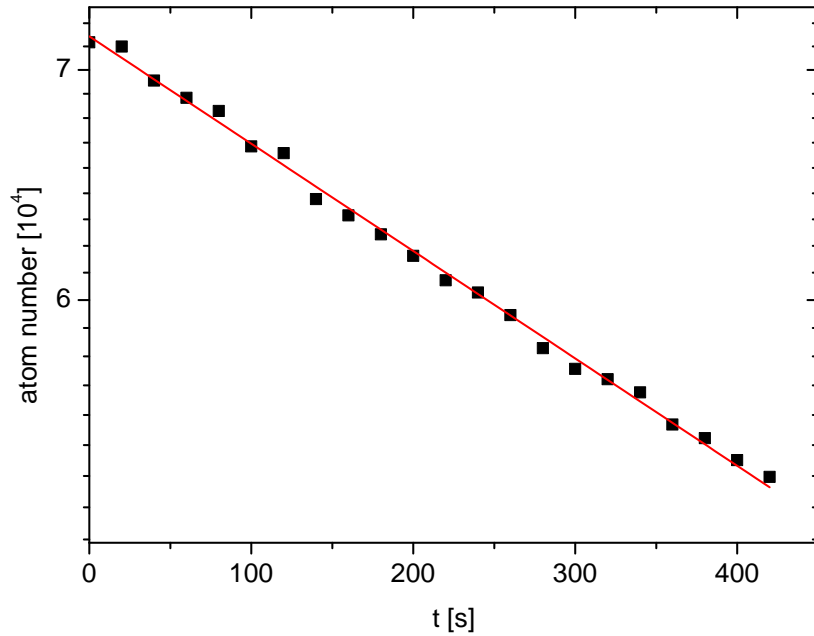


Figure 4.18: Loss of atoms from the MOT in the low density regime. The exponential decay yields a lifetime of $\tau = 1391$ s.

32bit counter in the experimental control that overflows after about 7 minutes. The measurement shown in figure 4.18 yields:

$$\tau = \frac{1}{R} = (1391 \pm 18) \text{ s} \approx 23 \text{ min} \quad (4.6)$$

which is far longer than any experimental cycle time we plan to use. A more detailed analysis of the MOT can be found in [\[Rie10\]](#).

5 Conclusion and Outlook

The aim of this work was to provide the basic tools and techniques that will be needed on the way to explore the physics mentioned at the beginning. The main foci were on the optical system (especially the frequency stabilization and tuneability), the Zeeman slower and the experimental control software. The following goals for the apparatus were reached:

- A laser system was built that is stable, robust and does not need much maintenance work to provide the light needed for the basic cooling techniques. It also provides light for more sophisticated imaging applications than we actually used in this basic setup.
- The constructed Zeeman slower allows for a very short experimental duty cycle as it slows the atom beam such that we can trap up to 10^9 atoms per second. This greatly helps future experiments because it will only take seconds to provide the experimentalist with a fresh implementation sample to do more advanced experiments with.
- The software to control the whole process is designed to allow for future extensions in both the hardware used in the laboratory and the software itself.

Together with the work [Rie10] this leads to a MOT filled with about 10^9 ^6Li atoms with a temperature in the order of the Doppler temperature. This leads to a phase space density of about 10^{-4} which is still 4 orders of magnitude away from what we want to achieve. But since the temperature we can reach with a MOT is fundamentally limited it is clear that we need other cooling schemes.

A prime example is **evaporative cooling**. To realize it we need a new type of atom trap where the atoms are not heated due to resonant light and one can tune the depth of the trap easily. A more detailed analysis of the atom-light interaction yields the following formulas for the so-called **dipole force**:

$$U_{\text{dipole}}(\mathbf{r}) = \frac{3\pi c^2}{2\omega_0^3} \left(\frac{\gamma}{\omega_0 - \omega} + \frac{\gamma}{\omega_0 + \omega} \right) I(\mathbf{r}) \quad (5.1)$$

$$\Gamma_{\text{sc}}(\mathbf{r}) = \frac{3\pi c^2}{2\hbar\omega_0^3} \left(\frac{\omega}{\omega_0} \right)^3 \left(\frac{\gamma}{\omega_0 - \omega} + \frac{\gamma}{\omega_0 + \omega} \right)^2 |I(\mathbf{r})| \quad (5.2)$$

Here the scattering rate scales like $\frac{I}{(\Delta\omega)^2}$ while the potential only scales like $\frac{I}{\Delta\omega}$. Therefore a trap with low scattering rate can be constructed by choosing far detuning and high intensity I . Since this trap would not be strong enough (typical trap depth \approx mK) to capture even the slowed atoms it will be loaded from the precooled atoms of the MOT. After this transfer the trap depth is slowly lowered which allows hot atoms to escape thus cooling the rest via rethermalization.

By letting strong far detuned laser beams interfere with each other one can shape different kinds of trapping potentials. As shown in figure 5.1 we can use them to form a flat two-dimensional trap or even a 2-D optical lattice.

When the optical lattice is in place we will also need an adequate imaging system. Therefore a specially designed objective is being manufactured with a resolution of 700 nm over a 200 μ m field of view. Since this objective is optimized for 671 nm and 1064 nm light it serves two purposes. Obviously we will be able to image the atoms with almost single site resolution but secondly we can shine additional light into the trap modifying the potential. With this setup (shown in figure 5.2) we aim to further explore the physics of the Hubbard model described in chapter 1 as well as other effects.

One prime example is the observation of anti-ferromagnetic ordering of fermions in a lattice [Lew07]. This effect is predicted by the Hubbard model but has not been observed so far because of the tremendous experimental requirements. However, with all the techniques mentioned this systems comes into reach of our apparatus.

Another interesting field of research is the three component Fermi gas in an optical lattice. As opposed to free space the three-body loss rate is suppressed by the Quantum Zeno effect, allowing research of new phases like the predicted color superfluid [Kan09] [Pri10].

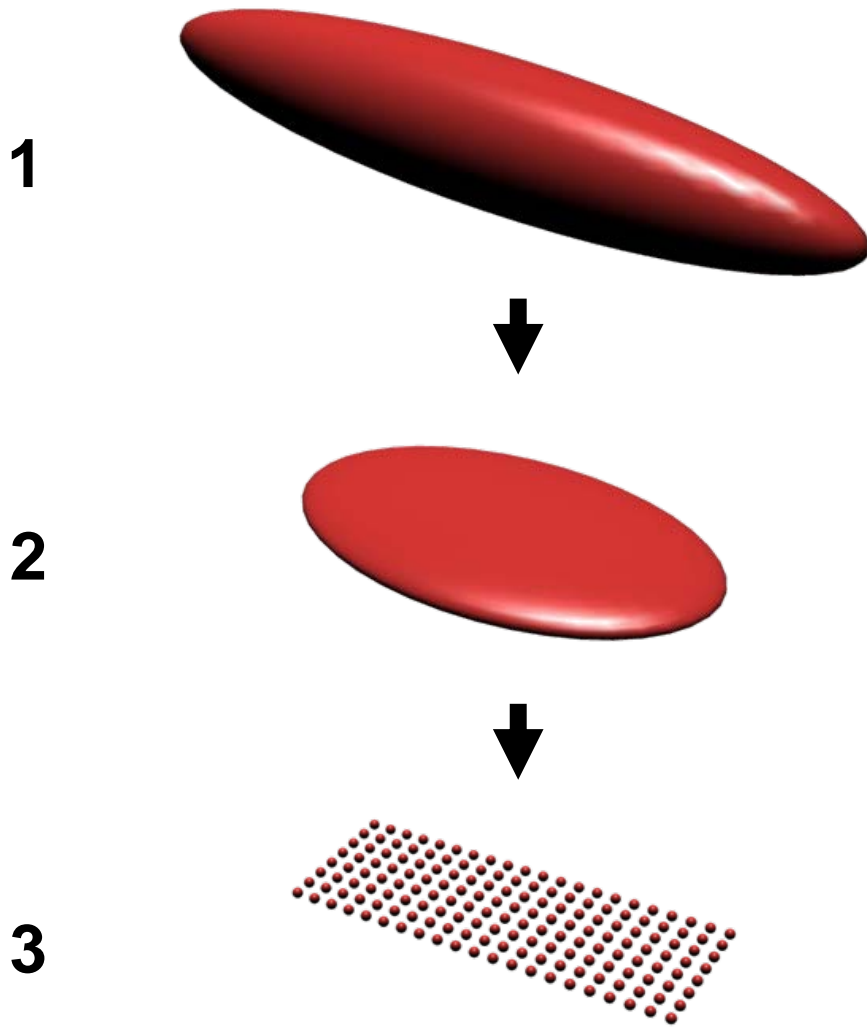


Figure 5.1: Different types of dipole traps. We start with a big cigar-shaped trap. With different beams we can form a flat pancake shaped trap which can ultimately be formed into an optical lattice.

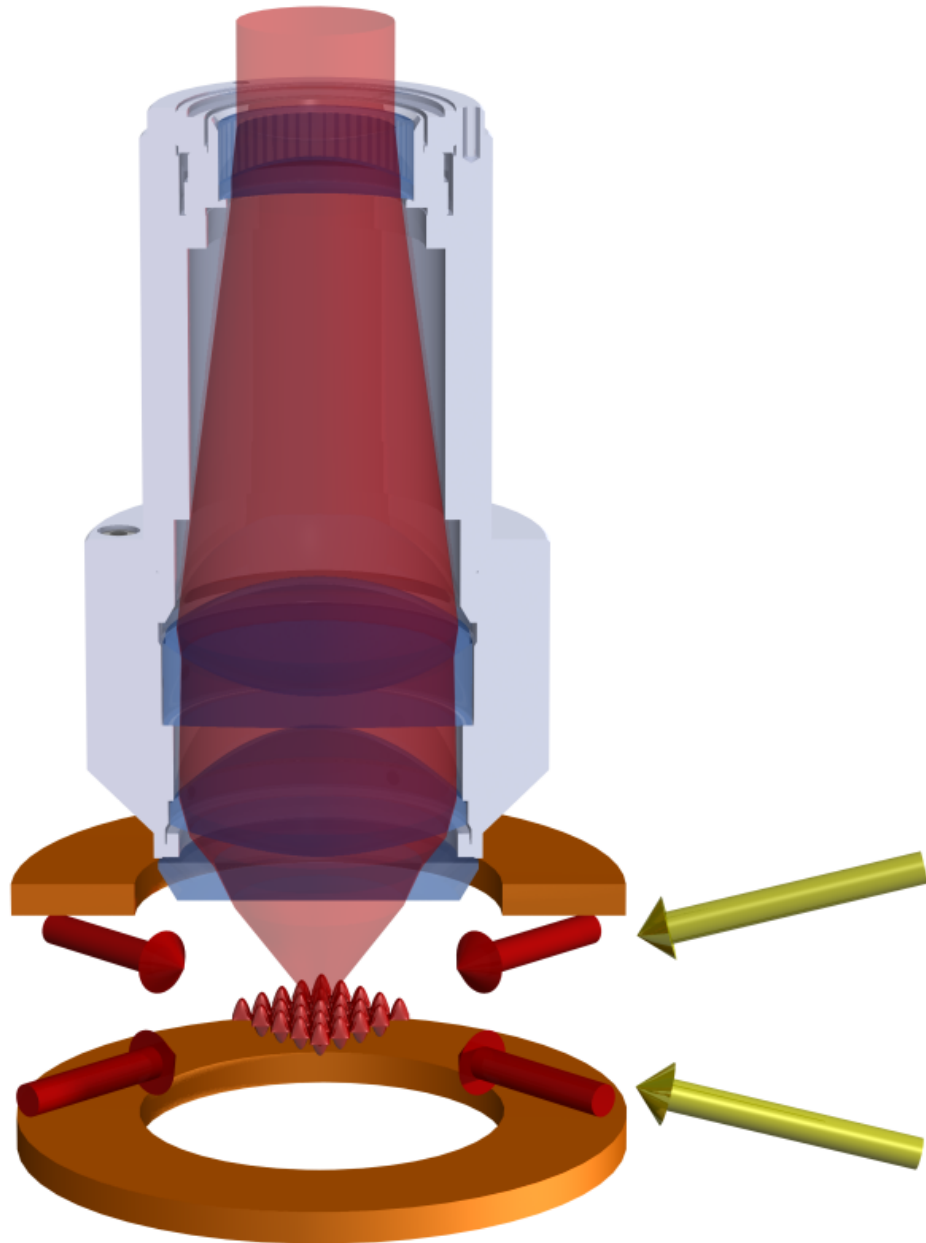


Figure 5.2: Beams involved in forming an optical lattice. The horizontal red beams form a 3-D lattice which is flattened by the yellow beams. Through the objective the lattice can be observed and manipulated.

Bibliography

- [And95] M. H. Anderson, J. R. Ensher, M. R. Matthews, C. E. Wieman, E. A. Cornell, *Observation of Bose-Einstein Condensation in a Dilute Atomic Vapor*, *Science* **269**(5221), 198–201 (1995).
- [Bar57] J. Bardeen, L. N. Cooper, J. R. Schrieffer, *Theory of Superconductivity*, *Phys. Rev.* **108**(5), 1175–1204 (Dec 1957).
- [Bla01] E. D. Black, *An introduction to Pound-Drever-Hall laser frequency stabilization*, *American Journal of Physics* **69**, 79–87 (Januar 2001).
- [Bos24] S. N. Bose, *Plancks Gesetz und Lichtquantenhypothese*, *Zeitschrift für Physik A Hadrons and Nuclei* **26**, 178–181 (1924), 10.1007/BF01327326.
- [Chu86] S. Chu, J. E. Bjorkholm, A. Ashkin, A. Cable, *Experimental Observation of Optically Trapped Atoms*, *Phys. Rev. Lett.* **57**(3), 314–317 (Jul 1986).
- [CT08] C. Cohen-Tannoudji, J. Dupont-Roc, G. Grynberg, *Optical Bloch Equations* (Wiley-VCH Verlag GmbH, 2008).
- [Dav95] K. B. Davis, M. O. Mewes, M. R. Andrews, N. J. van Druten, D. S. Durfee, D. M. Kurn, W. Ketterle, *Bose-Einstein Condensation in a Gas of Sodium Atoms*, *Phys. Rev. Lett.* **75**(22), 3969–3973 (Nov 1995).
- [Ein25] A. Einstein, *Quantentheorie des einatomigen idealen Gases*, in *Sitzungsberichte der Preussischen Akademie der Wissenschaften 1: 3* (1925).
- [Fes58] H. Feshbach, *A Unified Theory of Nuclear Reactions*, *Ann. Phys.* **5**, 337 (1958).
- [Geh03] M. E. Gehm, *Preparation of an Optically-Trapped Degenerate Fermi Gas of ^6Li : Finding the Route to Degeneracy*, Dissertation, Duke University (2003).
- [Gre92] W. Greiner, *Quantum Electrodynamics* (Springer, 1992).
- [Gre03] M. Greiner, C. A. Regal, D. S. Jin, *Emergence of a molecular Bose-Einstein condensate from a Fermi gas*, *Nature* **426**(6966), 537–540 (Dezember 2003).
- [Her08] I. V. Hertel, C.-P. Schulz, *Atome, Moleküle und optische Physik I* (Springer, 2008).

Bibliography

- [Hof02] W. Hofstetter, J. I. Cirac, P. Zoller, E. Demler, M. D. Lukin, *High-temperature superfluidity of fermionic atoms in optical lattices*, Phys. Rev. Lett. **89**, 220407–(2002).
- [Hub63] J. Hubbard, *Electron correlations in narrow energy bands*, Proc. R. Soc. Lond. A **276**, 238–257 (1963).
- [Jin99] D. S. Jin, B. DeMarco, *Onset of Fermi degeneracy in a trapped atomic gas*, Science **285(5434)**, 1703–1706 (1999).
- [Joc03] S. Jochim, M. Bartenstein, A. Altmeyer, G. Hendl, S. Riedl, C. Chin, J. Hecker Denschlag, R. Grimm, *Bose-Einstein Condensation of Molecules*, Science **302(5653)**, 2101–2103 (2003).
- [Jor08] R. Jordens, N. Strohmaier, K. Gunter, H. Moritz, T. Esslinger, *A Mott insulator of fermionic atoms in an optical lattice*, Nature **455(7210)**, 204–207 (September 2008).
- [Kan09] A. Kantian, M. Dalmonte, S. Diehl, W. Hofstetter, P. Zoller, A. J. Daley, *Atomic Color Superfluid via Three-Body Loss*, Phys. Rev. Lett. **103(24)**, 240401 (Dec 2009).
- [Ket08] W. Ketterle, M. W. Zwierlein, *Making, probing and understanding ultracold Fermi gases*, Nuovo Cimento Rivista Serie **31**, 247–422 (Mai 2008).
- [Lee06] P. A. Lee, N. Nagaosa, X.-G. Wen, *Doping a Mott insulator: physics of high-temperature superconductivity*, Rev. Mod. Phys. **78**, 17–85 (2006).
- [Lew07] M. Lewenstein, A. Sanpera, V. Ahufinger, B. Damskic, A. Send, U. Sen, *Ultracold atomic gases in optical lattices: mimicking condensed matter physics and beyond*, Adv. Phys. **56**, 234–379 (2007).
- [Met99] H. J. Metcalf, P. van der Straten, *Laser cooling and Trapping* (Springer, 1999).
- [Moe95] A. J. Moerdijk, B. J. Verhaar, A. Axelsson, *Resonances in ultracold collisions of ${}^6\text{Li}$, ${}^7\text{Li}$, and ${}^23\text{Na}$* , Phys. Rev. A **51(6)**, 4852–4861 (1995).
- [Mol97] P. A. Molenaar, P. van der Straten, H. G. M. Heideman, H. Metcalf, *Diagnostic technique for Zeeman-compensated atomic beam slowing: Technique and results*, Phys. Rev. A **55(1)**, 605–614 (Jan 1997).
- [Mot90] N. F. Mott, *Metal-Insulator Transitions* (Macmillan Publishers Limited. All rights reserved, 1990).
- [Nol06] W. Nolting, *Quantenmechanik - Methoden und Anwendungen* (Springer, 2006).

- [Pri10] A. Privitera, I. Titvinidze, S. Chang, S. Diehl, A. J. Daley, W. Hofstetter, *Loss-induced phase separation and pairing for 3-species atomic lattice fermions*, ArXiv e-prints (Oktober 2010).
- [Reg03] C. A. Regal, C. Ticknor, J. L. Bohn, D. S. Jin, *Creation of ultracold molecules from a Fermi gas of atoms*, *Nature* **424**(6944), 47–50 (Juli 2003).
- [Rie10] M. Ries, *A magneto-optical trap for the preparation of a three-component Fermi gas in an optical lattice*, diploma thesis, Universität Heidelberg (2010).
- [Sal91] B. E. A. Saleh, M. C. Teich, *Fundamentals of Photonics* (John Wiley & Sons Inc., 1991).
- [Sav98] T. A. Savard, *Raman-induced resonance imaging of trapped atoms*, Dissertation, DUKE UNIVERSITY (1998).
- [Sch99] U. Schünemann, H. Engler, R. Grimm, M. Weidemüller, M. Zielonkowski, *Simple scheme for tunable frequency offset locking of two lasers*, *Review of Scientific Instruments* **70**, 242–243 (Januar 1999).
- [Ser07] F. Serwane, *The setup of a Magneto Optical Trap for the preparation of a mesoscopic degenerate Fermi gas*, Masters Thesis, Universität Heidelberg (2007).
- [Ste99] J. Stenger, S. Inouye, M. R. Andrews, H.-J. Miesner, D. M. Stamper-Kurn, W. Ketterle, *Strongly Enhanced Inelastic Collisions in a Bose-Einstein Condensate near Feshbach Resonances*, *Phys. Rev. Lett.* **82**(12), 2422–2425 (Mar 1999).
- [Tru01] A. G. Truscott, K. E. Strecker, W. I. McAlexander, G. B. Partridge, R. G. Hulet, *Observation of Fermi Pressure in a Gas of Trapped Atoms*, *Science* **291**(5513), 2570–2572 (2001).
- [Zwi03] M. W. Zwierlein, C. A. Stan, C. H. Schunck, S. M. F. Raupach, S. Gupta, Z. Hadzibabic, W. Ketterle, *Observation of Bose-Einstein Condensation of Molecules*, *Phys. Rev. L* **91**(25) (2003).

Erklärung:

Ich versichere, dass ich diese Arbeit selbstständig verfasst und keine anderen als die angegebenen Quellen und Hilfsmittel benutzt habe.

Heidelberg, den _____

Unterschrift